https://doi.org/10.5194/essd-2024-315
Preprint. Discussion started: 25 October 2024

Open Access Earth System Science Data Discussions

A full-coverage satellite-based global atmospheric CO_2 dataset at 0.05° resolution from 2015 to 2021 for exploring global carbon dynamics

Zhige Wang[1,2], Ce Zhang[3,4], Kejian Shi[5], Yulin Shangguan[1], Bifeng Hu[6,7], Xueyao Chen[1], Danqing Wei[1,8], Songchao Chen[1,9*], Peter M. Atkinson[10,11], Qiang Zhang[2]

[1] *College of Environmental and Resource Sciences, Zhejiang University, Hangzhou 310058, China*

[2] *Ministry of Education Key Laboratory for Earth System Modeling, Department of Earth System Science, Tsinghua University, Beijing 100084, China*

[3] *School of Geographical Sciences, University of Bristol, Bristol BS8 1SS, UK*

[4] *UK Centre for Ecology & Hydrology, Library Avenue, Bailrigg, Lancaster LA1 4AP, UK*

[5] *School of Geographical Sciences, Faculty of Science and Engineering, University of Nottingham Ningbo China, Ningbo 315100, China*

[6] *Department of Land Resource Management, School of Public Finance and Public Administration, Jiangxi University of Finance and Economics, Nanchang, 330013, China*

[7] *Key Laboratory of Data Science in Finance and Economics, Jiangxi University of Finance and Economics, Nanchang, 330013, China*

[8] *Zhejiang Economic Information Center, Hangzhou, 310006, China*

[9] *ZJU-Hangzhou Global Scientific and Technological Innovation Center, Zhejiang University, Hangzhou 311215, China*

[10] *Lancaster Environment Centre, Lancaster University, Lancaster LA1 4YQ, UK*

[11] *Geography and Environment, University of Southampton, Highfield, Southampton SO17 1BJ, UK*

* Corresponding author: Songchao Chen (chensongchao@zju.edu.cn)

https://doi.org/10.5194/essd-2024-315
Preprint. Discussion started: 25 October 2024

Earth System Science Data Discussions
Open Access

Abstract

The irreversible trend for global warming underscores the necessity for accurate monitoring and analysis of atmospheric carbon dynamics on a global scale. Carbon satellites hold significant potential for atmospheric CO_2 monitoring. However, existing studies on global CO_2 are constrained by coarse resolution (ranging from 0.25° to 2°) and limited spatial coverage. In this study, we developed a new global dataset of column-averaged dry-air mole fraction of CO_2 (XCO_2) at 0.05° resolution with full coverage using carbon satellite observations, multi-source satellite products, and an improved deep learning model. We then investigated changes in global atmospheric CO_2 and anomalies from 2015 to 2021. The reconstructed XCO_2 products show a better agreement with Total Carbon Column Observing Network (TCCON) measurements, with R^2 of 0.92 and RSME of 1.54 ppm. The products also provide more accurate information on the global and regional spatial patterns of XCO_2 compared to origin carbon satellite monitoring and previous XCO_2 products. The global pattern of XCO_2 exhibited a distinct increasing trend with a growth rate of 2.32 ppm/year, reaching 414.00 ppm in 2021. Globally, XCO_2 showed obvious spatial variability across different latitudes and continents. Higher XCO_2 concentrations were primarily observed in the Northern Hemisphere, particularly in regions with intensive anthropogenic activity, such as East Asia and North America. We also validated the effectiveness of our XCO_2 products in detecting intensive CO_2 emission sources. The XCO_2 dataset is publicly accessible on the Zenodo platform at https://doi.org/10.5281/zenodo.12706142 (Wang et al., 2024). Our findings represent a promising advancement in monitoring carbon emission across various countries and enhancing the understanding of global carbon dynamics.

Keywords: Atmospheric carbon dioxide; Satellite carbon monitoring; Deep learning; OCO-2/3

1. Introduction

Carbon dioxide (CO_2) is a primary greenhouse gas (GHG). Anthropogenic activities and land use change since the industrial revolution have led to a marked increase in atmospheric CO_2, which is widely considered to be a major contributor to

https://doi.org/10.5194/essd-2024-315
Preprint. Discussion started: 25 October 2024

climate change, reaching a record-high of 414.71 parts per million (ppm) in 2021 (Friedlingstein et al., 2022). The damaging global climate change caused by atmospheric increases in CO_2 is severe and irreversible (IPCC, 2023; Kemp et al., 2022; Solomon et al., 2009). Consequently, the Paris Agreement announced to hold "the increase in the global average temperature to well below 2°C above pre-industrial levels" and pursue efforts "to limit the temperature increase to 1.5°C above pre-industrial levels." It was also determined that the joined parties should submit their nationally determined contributions (NDCs) to reduce CO_2 emissions.

Accurate monitoring of atmospheric CO_2 concentrations is crucial for measuring global CO_2 emissions mitigation as well as characterizing terrestrial carbon change. Currently, ground-based and airborne platform-based atmospheric CO_2 observation networks, such as the Total Carbon Column Observing Network (TCCON, https://tccondata.org/), are capable of providing CO_2 measurements with high accuracy (Petzold et al., 2016; Wunch et al., 2011, 2010). However, these observation networks are insufficient to fully explore the spatiotemporal patterns of atmospheric CO_2 at a global scale. The launch of a series of carbon observation satellites in recent years has provided favorable opportunities for continuous and large-scale atmospheric CO_2 observation (Buchwitz et al., 2015; Hammerling et al., 2012). The Scanning Imaging Absorption Spectrometer for Atmospheric Chartography (SCIAMACHY) onboard EnviSat was one of the first instruments to monitor the atmospheric column-averaged dry-air mole fraction of CO_2 (XCO_2) (Bovensmann et al., 1999). The Greenhouse Gases Observing Satellite (GOSAT) launched by Japan utilized the Thermal And Near-Infrared Sensor for carbon Observation (TANSO) instrument to monitor XCO_2 globally, providing products with a spatial resolution of 10 km every three days (Butz et al., 2011). The Orbiting Carbon Observatory-2 (OCO-2) and OCO-3 launched by NASA provide XCO_2 measurements at a finer spatial resolution (Crisp et al., 2017; Eldering et al., 2017). These sensors are considered among the best for XCO_2 observation, featuring larger overlapping swaths that cover areas of ~20×80 km² and exhibiting the least retrieval absolute bias, measuring less than 0.4 ppm (Eldering et al., 2019; Taylor et al., 2020). However, the narrow swath of the sensor can only cover limited spatial areas, and caused by the cloud and aerosol contaminations, the data from OCO-2/3 always contain large amount of missing values (Taylor et al., 2016; Crisp et al., 2017). These limitations obstacle the better understanding of the atmosphere-land carbon cycle over large spatial scale based on satellite observation.

https://doi.org/10.5194/essd-2024-315
Preprint. Discussion started: 25 October 2024

Consequently, several studies have concentrated on generating spatially continuous XCO_2 products based on satellite observations (He et al., 2022; Siabi et al., 2019; Zhang and Liu, 2023). One potential solution is the application of diverse interpolation methods (He et al., 2020; Zeng et al., 2014). Hammerling et al. (2012) mapped the global distribution of CO_2 based on OCO-2 and the geostatistical method. Zeng et al. (2014) developed a gap-filling model based on the space-time kriging to obtain gap-filled GOAST XCO_2 data in China. However, their results encounter large uncertainty in regions with sparse data coverage, due to algorithmic constraints and the coarse spatial resolution of the original data. Recently, data fusion techniques have gained recognition as an effective method for obtaining full-coverage XCO_2 data (Sheng et al., 2023; He et al., 2022; Siabi et al., 2019; Zhang and Liu, 2023). These techniques can be broadly categorized into two groups based on their underlying principles. The first category leverages the spatiotemporal correlation inherent in multi-source XCO_2 data, fusing them based on this spatiotemporal information (Wang et al., 2023; Sheng et al., 2023). For instance, Wang et al. (2023) introduced a spatiotemporal self-supervised fusion model and generate seamless global XCO_2 data at a spatial resolution of 0.25°. The second category is regression-based methods, which aim to fill the gap in XCO_2 data by capturing the nonlinear relationship between multi-source XCO_2 measurements and related covariates (He et al., 2022; Siabi et al., 2019; Zhang and Liu, 2023). This category includes a range of specific methodologies, from traditional statistical and geostatistical models to advanced machine learning models. Siabi et al (2019) employed the Artificial Neural Network (ANN) to establish correlation between XCO_2 and eight environmental variables. Zhang and Liu (2023) utilized the convolution neural networks (CNN) coupled with attention mechanisms to produce full-coverage XCO_2 data across China.

Despite significant efforts to generate seamless XCO_2 products using satellite observations, several challenges and limitations persist. Firstly, due to the sparse distribution of satellite XCO_2 data, previous studies have relied on assimilation and reanalysis XCO_2 data as covariates. This reliance often results in final products that closely mirror the assimilation and reanalysis results, leading to an oversmoothed distribution that undermines the high-resolution advantages of satellite data. Furthermore, most studies that employ regression models to estimate full-coverage XCO_2 are limited to regional or national scales due to the weak transferability of these

https://doi.org/10.5194/essd-2024-315
Preprint. Discussion started: 25 October 2024

Open Access Earth System Science Data Discussions

models. Consequently, there is a scarcity of research investigating global patterns of XCO_2 based on statistical models. Additionally, the current generation of XCO_2 products typically features a coarse spatial resolution, ranging from approximately 0.25° to 2°. In conclusion, there is an urgent need to develop global full-coverage XCO2 products with a fine spatial resolution. This development should leverage satellite carbon monitoring and advanced methods that exhibit spatiotemporal transferability to overcome the aforementioned limitations.

In this study, we leveraged time-series OCO-2/3 XCO_2 data and various related environmental variables retrieved from multi-source satellites to generate global full-coverage XCO_2 products. The advanced deep learning method was adopted to model time-series XCO_2 and incorporate terrestrial flux, anthropogenic flux and climatic impacts into the parameterization process. Our XCO_2 products achieved full global coverage with a spatial resolution of 0.05° and a monthly temporal resolution from 2015 to 2021. We also validated our XCO_2 products against in-situ XCO_2 data and other XCO_2 products. Based on our high-resolution products, we explored the spatial and temporal pattern of atmospheric CO_2 globally and identified regions with intense CO_2 emission. Our findings aim to enhance the understanding of carbon dynamics on a global scale through data reconstruction and analysis.

2. Materials and methods

In this study, we utilized Google Earth Engine (GEE) to integrate OCO-2/3 XCO_2 data and multiple environmental variables as data inputs. In addition, the attention-based Bidirectional Long Short-Term Memory (At-BiLSTM) model was trained for building the relationship between OCO-2/3 XCO_2 and the related environmental variables. Then, we reconstructed the global monthly XCO_2 and validated the accuracy of the products against TCCON XCO_2 data and the original OCO-2/3 XCO_2 data. We also analyzed the spatial and temporal variation of XCO_2 over the globe and detect the intense CO_2 emission regions. The methodology framework is shown in Fig.1.

https://doi.org/10.5194/essd-2024-315
Preprint. Discussion started: 25 October 2024

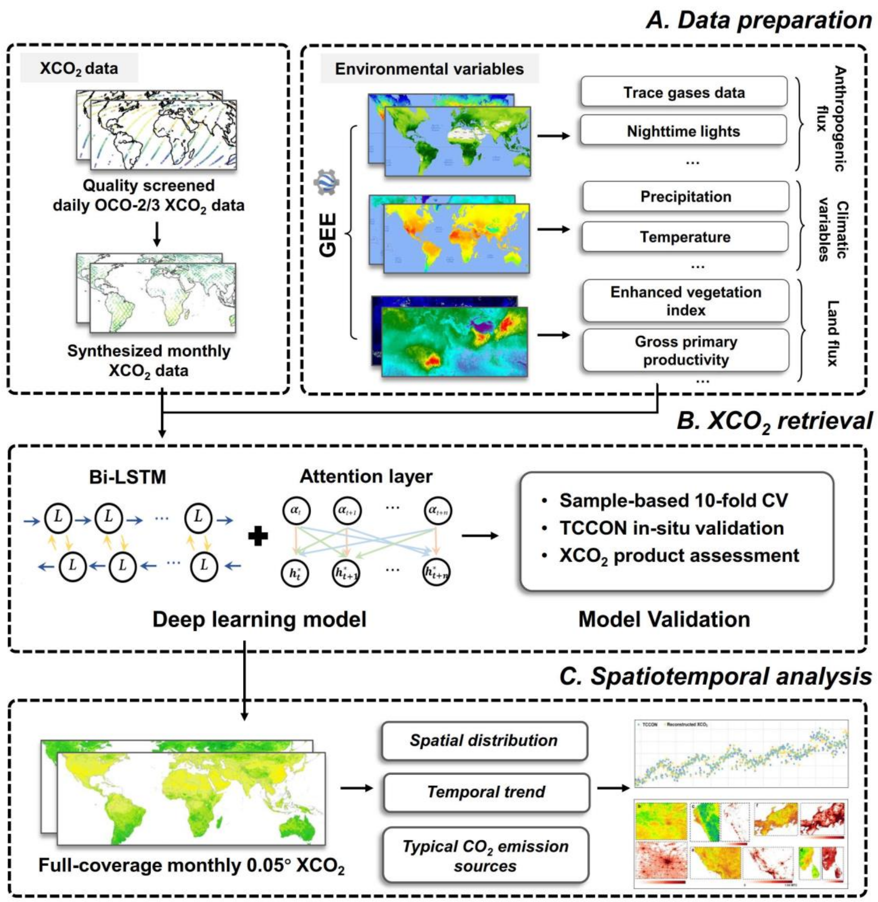

Figure 1. The workflow for mapping and exploring global XCO_2 dynamics and drivers.

2.1 Datasets

2.1.1 OCO XCO_2 data

In this study, we utilized the satellite-based XCO_2 data from OCO-2 and OCO-3, covering the period from December 2014 to December 2021. The OCO-2/3 measure at three near-infrared wavelength bands, that are 0.76 μm Oxygen A-band, 1.61 μm weak CO_2, and 2.06 μm strong CO_2 bands (Crisp et al., 2004). The full physics retrieval algorithm was used to retrieve the XCO_2 based on the observation of the two satellites (Crisp et al., 2021). Previous studies (Taylor et al., 2023) suggested that the OCO-2 and OCO-3 XCO_2 measurements are in broad consistency and can therefore be used together in scientific analyses. The OCO-3 Level 2 XCO_2 Lite version 10.4r data (OCO3_L2_Lite_FP V10.4r) from 2020 to 2021 and the OCO-2 Level 2 XCO_2 Lite

https://doi.org/10.5194/essd-2024-315
Preprint. Discussion started: 25 October 2024

version 11r (OCO2_L2_Lite_FP V11r) from 2015 to 2019 were downloaded from Goddard Earth Sciences Data and Information Services Center (GES DISC, https://disc.gsfc.nasa.gov/). The products were aggregated as a daily file (Fig. 2) with a spatial resolution of 2.25 km × 1.29 km (O'Dell et al., 2018). The XCO_2 data were quality filtered, and only good-quality data (i.e., xco2_quality_flag=0) were considered. To generate the monthly products with a spatial resolution of 0.05° × 0.05°, we converted the daily data to monthly data by averaging the sparse XCO_2 data within a range of 0.05° × 0.05° over one month.

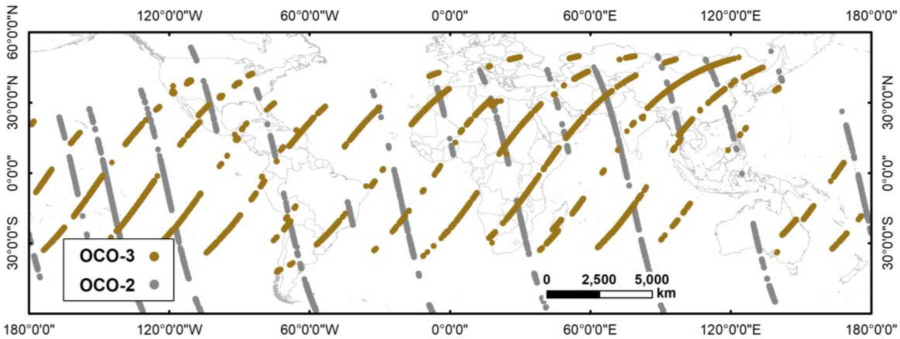

Figure 2. Footprints of OCO-2 and OCO-3 XCO_2 data on 20th January 2018 and 4th December 2021 (with quality filtering) as examples.

2.1.2 TCCON XCO_2 data

The Total Carbon Column Observing Network (TCCON) is a global network for measuring atmospheric CO_2, methane (CH_4), carbon monoxide (CO) and other trace gases in the atmosphere. The XCO_2 data from TCCON were demonstrated to have high accuracy with ~0.2% of XCO_2 (Wunch et al., 2011). Consequently, the data have been used widely for the validation of satellite observations such as OCO-2, OCO-3 and GOSAT (Deng et al., 2016; Wunch et al., 2017). In this research, we used the GGG2014 and GGG2020 datasets from 23 sites (Fig. 3 and Table 1) around the world to validate the reconstructed XCO_2 products.

https://doi.org/10.5194/essd-2024-315
Preprint. Discussion started: 25 October 2024

Open Access Earth System Science Data Discussions

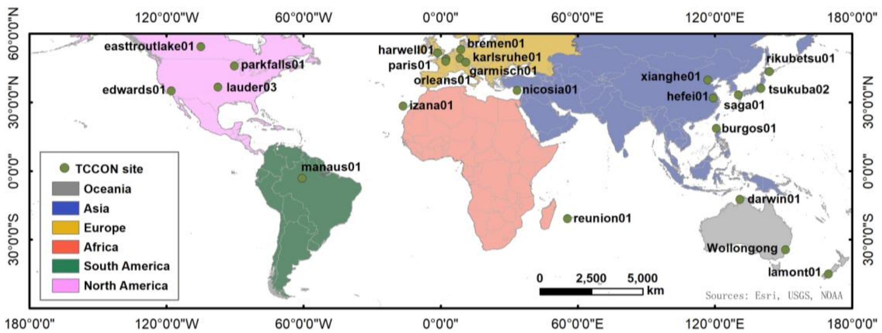

Figure 3. The locations of the TCCON sites.

Table 1. The information on the TCCON *in situ* stations.

ID	Site name	Longitude	Latitude	Start date	End date
1	saga01 (JP)	130.29	33.24	2011-07-28	2021-06-30
2	xianghe01 (PRC)	116.96	39.80	2018-06-14	2022-04-09
3	burgos01 (PH)	120.65	18.53	2017-03-03	2021-08-20
4	harwell01 (UK)	-1.32	51.57	2021-05-30	2022-05-22
5	bremen01 (DE)	8.85	53.10	2009-01-06	2021-06-24
6	tsukuba02 (JP)	140.12	36.05	2014-03-28	2021-03-31
7	lauder03 (NZ)	-97.49	36.60	2018-10-02	2022-11-14
8	edwards01 (US)	-117.88	34.96	2013-07-20	2022-12-25
9	nicosia01 (CY)	33.38	35.14	2019-09-06	2021-06-01
10	izana01 (ES)	-16.5	28.31	2014-01-02	2022-10-31
11	orleans01 (FR)	2.11	47.96	2009-09-06	2022-04-24
12	hefei01 (PRC)	119.17	31.90	2015-11-02	2020-12-31
13	easttroutlake01 (CA)	-104.99	54.35	2016-10-03	2022-08-13
14	karlsruhe01 (DE)	8.44	49.10	2014-01-15	2023-01-20
15	paris01 (FR)	2.36	48.85	2014-09-23	2022-03-28
16	garmisch01 (DE)	11.06	47.48	2007-07-18	2021-10-18
17	rikubetsu01 (JP)	143.77	43.46	2014-06-24	2021-06-30
18	lamont01 (US)	169.68	-45.04	2011-04-16	2022-12-19
19	reunion01 (RE)	55.48	-20.90	2015-03-01	2020-07-18
20	darwin01 (AU)	130.93	-12.46	2005-08-28	2020-04-30
21	Wollongong (AU)	150.88	-34.41	2008-06-26	2020-06-30
22	Manaus01(BR)	-60.60	-3.21	2014-09-30	2015-07-27
23	parkfalls01 (US)	-90.27	45.94	2004-06-02	2020-12-29

https://doi.org/10.5194/essd-2024-315
Preprint. Discussion started: 25 October 2024

JP: Japan, DE: Germany, FI: Finland, FR: French, RE: Réunion Island, AU: Australia, BR: Brazil; US: United States, PRC: People's Republic of China, NO: Norway, CY: Cyprus, NZ: New Zealand, PH: Philippines, UK: United Kingdom, CA: Canada.

2.1.3 Environmental variables

In the selection of environmental variables, our primary focus was on processes within the terrestrial carbon cycle. The carbon cycle on land can be conceptualized as two flux exchange processes influenced by the climatic conditions (Fig. 4). The CO_2 in the atmosphere is fixed by vegetation photosynthesis and the carbon is released back into the atmosphere by respiration and disturbance processes (Beer et al., 2010; Pan et al., 2011). The carbon fluxes through these processes we considered as the land flux. Since Industrial Era, anthropogenic carbon from land use change (e.g., deforestation) and fossil fuels and cement become important parts of atmospheric CO_2 (Friedlingstein et al., 2010), which we considered as the anthropogenic flux. Meanwhile, the two processes are directly or indirectly driven by the climatic features (Sitch et al., 2015; Chen et al., 2021). Consequently, we explored the potential drivers of XCO_2 from the perspective of the carbon cycle at atmosphere-land interface. Multiple satellite products and reanalysis data from three aspects (i.e., land flux, anthropogenic flux and climatic impacts) were selected to consider their various effects on the XCO_2.

https://doi.org/10.5194/essd-2024-315
Preprint. Discussion started: 25 October 2024

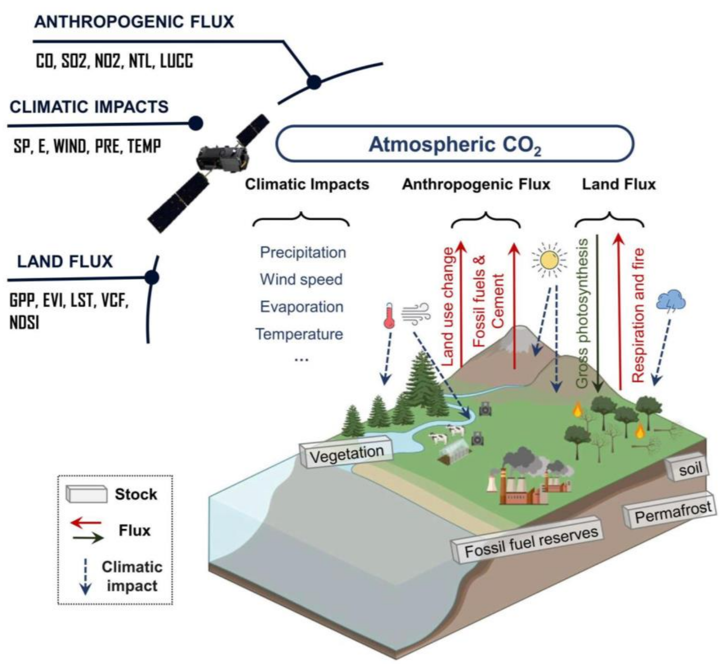

Figure 4. Simplified illustration of the global carbon cycle on land (referring to IPCC 2023). Noting that the carbon cycle in the ocean was not considered in our study and we only focused on the fast exchange fluxes. The slow carbon exchanges (e.g., chemical weathering, volcanic emissions) which are generally assumed as relatively constant over the last few centuries (Sundquist, 1986), were not included here.

The key factors selected related to the land flux included gross primary productivity (GPP), enhanced vegetation index (EVI), land surface temperature (LST), vegetation continuous fields (VCF), and normalized difference snow index (NDSI). These products are all obtained from the Moderate Resolution Imaging Spectroradiometer (MODIS), which has been operated for over 20 years and produced various satellite products with fine spatial resolution and accuracy. The EVI and NDSI were converted to monthly data using the maximum value composite (MVC) method. The GPP and LST were converted to monthly data by the averaging method.

The rising anthropogenic activities have greatly influenced atmospheric CO_2 (Friedlingstein et al., 2022). In this study, five anthropogenic factors, including land use/cover change (LUCC), nighttime lights (NTL), and three trace gases (i.e., sulfur dioxide (SO_2), nitrogen dioxide (NO_2), and carbon monoxide (CO)) were selected. The LUCC was obtained from MODIS MCD12Q1 with a spatial resolution of 500 m. The monthly Suomi National Polar-orbiting Partnership-Visible Infrared Imaging

https://doi.org/10.5194/essd-2024-315
Preprint. Discussion started: 25 October 2024

Open Access Earth System Science Data Discussions

Radiometer Suite (NPP-VIIRS) day/night band (DNB) NTL products (spatial resolution of 15 arc-second, ~500 m) were obtained from the Earth Observation Group (EOG) of the Colorado School of Mines. We also used the SO_2, NO_2 and CO products from the TROPOspheric Monitoring Instrument (TROPOMI) onboard Sentinel-5 Precursor (S5P), a global air monitoring satellite for the Copernicus mission. The data were also converted to the same temporal resolution (i.e., monthly).

The selected climatic factors affecting XCO_2 were surface pressure (SP), 10 m wind speed (WS), precipitation flux (PRE), 2 m air temperature (Temp), and total evaporation (E). These data are from the reanalysis products (Hersbach et al., 2020) developed at the European Center for Medium Weather Forecasting (ECMWF, https://www.ecmwf.int/). The WS is calculated using the products of 10 m wind components of U and V. All data were converted to monthly time-series. The bilinear interpolation approach was used to convert the data at different spatial resolutions to 1 km resolution. The data preprocessing was conducted on GEE, R and ArcGIS 10.3. Details of these products are listed in Table 2.

Table 2. Ancillary variables selected in this study.

Variables	Spatial resolution	Temporal resolution	Product names	Category
GPP	500 m	8-day	MOD17A2H	
EVI	1 km	16-day	MOD13A2	Land flux-related
LST	1 km	daily	MOD11A1	
VCF	250 m	annual	MOD44B	
NDSI	500 m	daily	MOD10A1	
LUCC	500 m	annual	MCD12Q1	
NTL	15 arc-second	monthly	VNP46A2	Anthropogenic flux-related
SO_2			OFFL/L3_SO_2	
NO_2	~1 km	daily	OFFL/L3_NO_2	
CO			OFFL/L3_CO	
SP				
E				
Wind-v	~10 km	monthly	ERA5-Land	Climatic impacts
Wind-u				
Pre				
Temp				

https://doi.org/10.5194/essd-2024-315
Preprint. Discussion started: 25 October 2024

2.2 Deep learning-based XCO_2 reconstruction

Given the complexity temporal dependence and nonlinear relationship between XCO_2 and the environmental variables, we selected the At-BiLSTM model to relate the XCO_2 data with the 16 response variables affecting atmospheric CO_2, and further reconstruct the XCO_2 data at a fine spatial resolution. The equation to reconstruct XCO_2 data in this research can be denoted as:

$$XCO_{2(i)} = f_{bilstm}([\mathrm{LF}_{i,j}], [\mathrm{AF}_{i,j}], [\mathrm{CI}_{i,j}]) \quad (1)$$

$$= f_{bilstm}([\mathrm{GPP}_i, \mathrm{EVI}_i, \mathrm{LST}_i, \mathrm{VCF}_i, \mathrm{NDSI}_i], [\mathrm{LUCC}_i, \mathrm{NTL}_i, \mathrm{SO}_{2i}, \mathrm{NO}_{2i}, \mathrm{CO}_i], [\mathrm{SP}_i, E_i, \mathrm{WU}_i, \mathrm{WV}_i, \mathrm{PRE}_i, \mathrm{TEMP}_i]) \quad (2)$$

where $XCO_{2(i)}$ denotes the aggregated monthly atmospheric CO_2 concentration at grid cell i, $[\mathrm{LF}_{i,j}]$, $[\mathrm{AF}_{i,j}]$, and $[\mathrm{CI}_{i,j}]$ denote the variables from land flux, anthropogenic flux, and climatic impacts, respectively. And j denotes the number of variables in each category. The f_{bilstm} represents the estimation model of each grid cell at the spatial resolution of 0.05°.

The LSTM model is a variant of RNN that excels in processing time-series data (Hochreiter and Schmidhuber, 1997; Graves et al., 2005). It has been utilized extensively for prediction of remote sensing data. Each LSTM cell includes an input gate, a forget gate and an output gate. The forget gate f_t determines which information from the previous time step to forget, the input gate i_t governs the selective storage of the data in current time step, and the output from forget gate f_t and input gate i_t are combined in the cell state C_t. Lastly, the output gate o_t controls the flow of information from the cell state to the next time step. These gate structures effectively manage the flow of information within the LSTM, enabling it to capture the temporal dependencies present in the data (Yuan et al., 2020; Su et al., 2021). Bidirectional LSTM consists of two directional LSTM, in which the data flows forward and backward. Then we defined a multi-dimensional attention layer behind the BiLSTM to focus on more critical variables and give them higher weights (Bahdanau et al., 2016). In the attention layer, we adopted the full connection layer and softmax activation function to calculate the attention weight of each time step.

The At-BiLSTM consists of one input layer, three Bidirectional LSTM layers, one attention layer, one dropout layer to prevent overfitting, and one fully connected layer (i.e., dense layer) for the final output. The mean square error is used as the loss function. The number of network units, batch size, learning rate and activation function

https://doi.org/10.5194/essd-2024-315
Preprint. Discussion started: 25 October 2024

hyperparameters were all tuned in model fitting. All data were normalized using the mean and standard deviation of the dataset. The model was built using the deep learning API Keras in Python.

In this study, we adopted the sample-based cross-validation (CV) method to evaluate the model performance and the in-situ validation to assess the accuracy of reconstructed XCO_2 products. We also compared the reconstructed XCO_2 products with the original OCO XCO_2 products and the CAMS-EGG4 GHGs data. Four metrics, including coefficient of determination (R^2), root mean squared error (RMSE), mean absolute error (MAE) and mean bias, were calculated as follow, to assess the model performance.

$$R^2 = 1 - \frac{\sum_{i=1}^{n}(y_i - f_i)^2}{\sum_{i=1}^{n}(y_i - \bar{y})^2} \tag{3}$$

$$RMSE = \sqrt{\frac{\sum_{i=1}^{n}(y_i - f_i)^2}{n}} \tag{4}$$

$$MAE = \frac{\sum_{i=1}^{n}|(f_i - y_i)|}{n} \tag{5}$$

where n is the total number of data samples, and f_i, y_i are the observed results and model-estimated results, respectively.

3. Results

3.1 Validation of the reconstructed XCO_2 product

3.1.1 Model validation results

Given the distinct seasonal variation in XCO_2 concentrations, we conducted the sample-based CV to evaluate the model performance during different seasons (Fig. 5). The model demonstrated high accuracy across all seasons, with R^2 values exceeding 0.81, MAE less than 0.73 ppm, and RMSE less than 1.09 ppm. The model performed better in spring and summer, as indicated by the densest cluster of points being closest to the 1:1 line. Conversely, the model performed worst in winter, when photosynthesis is weakest, leading to greater estimation deviation. These variations are likely influenced by the ecosystem CO_2 exchange during different seasons. Overall, the model effectively captured the seasonal variation of XCO_2 and provided unbiased XCO_2 estimations.

https://doi.org/10.5194/essd-2024-315
Preprint. Discussion started: 25 October 2024

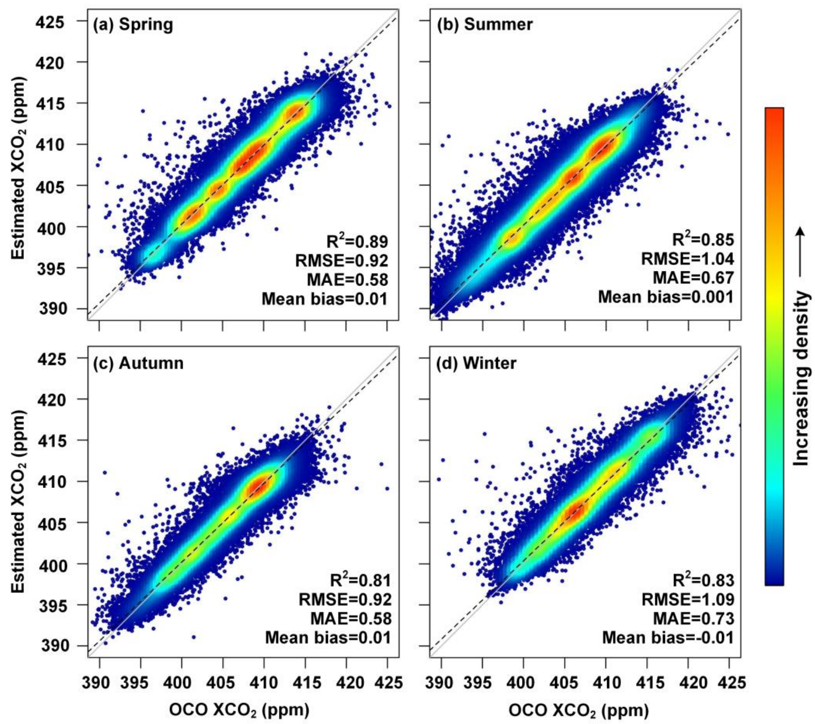

Figure 5. (a) Density scatterplots of sample-based CV results during different seasons. The proportion of the number of points is represented as the color of the points. The black dashed lines and grey solid lines denote the linear regression fitted lines and the 1:1 line, respectively. The R^2, RMSE (ppm), MAE (ppm), and mean bias (ppm) are provided.

We further validated the model performance across different continents. Table 3 presents the validation results for six continents. The model performance varied across continents. Notably, the model achieved the highest accuracy in Africa and Europe, with R^2 of 0.80 and 0.81, and RMSE values of 1.02 and 1.14 ppm, respectively. In contrast, the model demonstrated relatively low accuracy in Oceania and South America, both located in the southern hemisphere. Despite this, the RMSE of the model in these continents were 1.21 and 0.66 ppm, respectively, indicating that the model maintained acceptable estimation accuracy in these regions.

https://doi.org/10.5194/essd-2024-315
Preprint. Discussion started: 25 October 2024

Table 3. Model performance in different continents.

	R^2	RMSE (ppm)	MAE (ppm)	Mean bias (ppm)
Africa	0.80	1.02	0.70	-0.009
Asia	0.73	1.27	0.85	0.002
Europe	0.81	1.14	0.77	-0.030
North America	0.73	1.26	0.83	-0.020
South America	0.59	1.22	0.86	-0.012
Oceania	0.67	0.66	0.4	0.051

3.1.2 In situ validation results

The TCCON in situ XCO_2 data were adopted for validating the accuracy of the reconstructed XCO_2 over the globe. The validation results for our reconstructed XCO_2 and the origin OCO-2/3 XCO_2 are displayed in Fig. 6. The two XCO_2 data showed similar precision with the R^2 value of 0.91 and 0.92, respectively (Fig. 6c-d). While the reconstructed XCO_2 greatly increases the data coverage with the validation sample increasing from 578 to 1432. Meanwhile, the reconstructed XCO_2 has a smaller RMSE and MAE with values of 1.72 and 1.3 ppm, respectively, compared with the OCO XCO_2. These results indicate that the reconstructed XCO_2 had a closer agreement with TCCON XCO_2. We also displayed the mean bias of OCO and reconstructed XCO_2 in each TCCON site (Fig. 6a-b). As shown in Fig. 6a, the OCO-2/3 observation tend to overestimate the XCO_2, while the reconstructed XCO_2 could amend the underestimation of OCO XCO_2. Over 68% of the validation sites of reconstructed XCO_2 had a mean bias less between ± 0.4 ppm. Given the orbital constraints of the ISS (Eldering et al., 2019), OCO-3 measurements were restricted to latitudes below ± 52°. Consequently, substantial missing values of OCO XCO_2 data were shown around 50°N, introducing a potential bias. In contrast, the reconstructed XCO_2 effectively solves this problem and demonstrates markedly enhanced performance.

https://doi.org/10.5194/essd-2024-315
Preprint. Discussion started: 25 October 2024

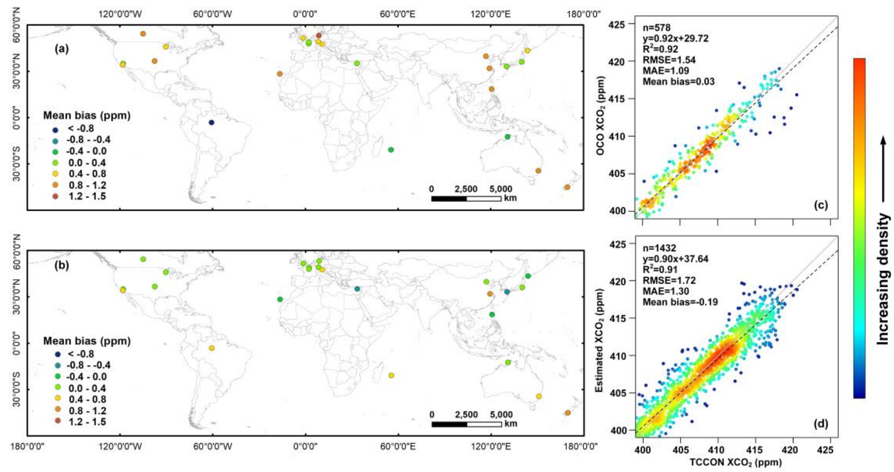

Figure 6. The mean bias of the (a) OCO observed XCO_2, and (b) reconstructed XCO_2 against global TCCON XCO_2; (c) density scatterplots of the validation results for OCO observed XCO_2, and (d) reconstructed XCO_2 against the TCCON XCO_2. The proportion of the number of points is represented as the color of the points. The number of samples *n*, linear regression relation, R^2, RMSE (ppm), MAE (ppm), and mean bias are provided.

Fig. 7 shows the individual in situ validation results of the reconstructed XCO_2 against TCCON site in different continents (except Antarctica). The sample numbers are varying in different sites due to the observation constraints, while the validation results from all sites showed satisfying performance. The R^2 for all sites are over 0.88 and the MAE are less than 1.46 ppm. The reconstructed XCO_2 data performs the best in sites lauder03 and karlsruhe01, which located in North America and Europe, respectively. While the reconstructed XCO_2 performed worst in saga01 which located in Asia, potentially due to the high CO_2 concentrations in these regions. Overall, the reconstructed XCO_2 showed high consistency with the in situ XCO_2 observation in different regions over the globe.

https://doi.org/10.5194/essd-2024-315
Preprint. Discussion started: 25 October 2024

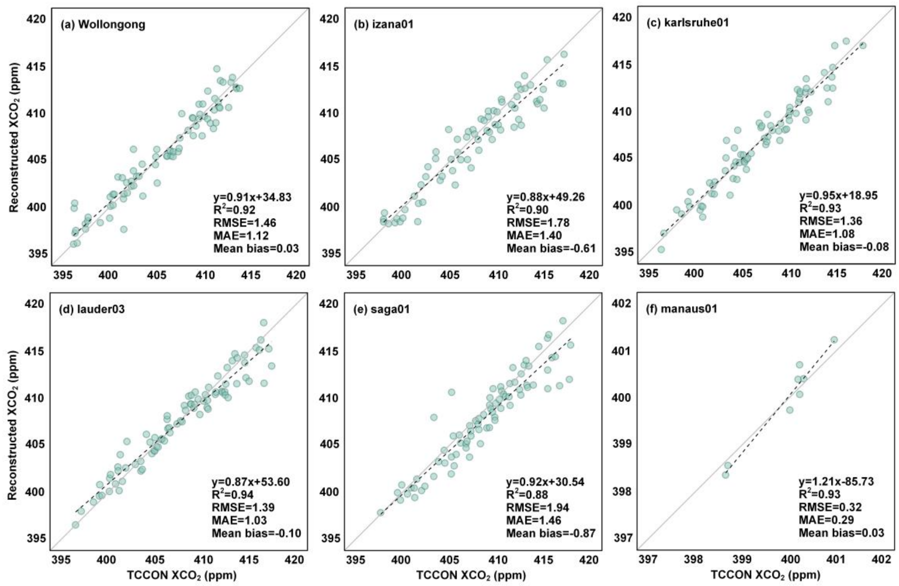

Figure 7. Scatterplots of the TCCON in situ validation results of the reconstructed XCO_2 on different TCCON sites over the globe.

To assess the performance of our reconstructed XCO_2 in temporal analysis, we compared the time series for monthly OCO-2/3, reconstructed and TCCON XCO_2 data from December 2014 to December 2021. As depicted in Fig. 8, the reconstructed XCO_2 exhibits similar temporal patterns compared to the TCCON data, with the mean RMSE and MAE of 1.47 and 1.07 ppm. While the OCO-2/3 XCO_2 exhibits some overestimation for high values and underestimation for low values compared with TCCON data. In contrast, the reconstructed XCO_2 provided more stable estimate results.

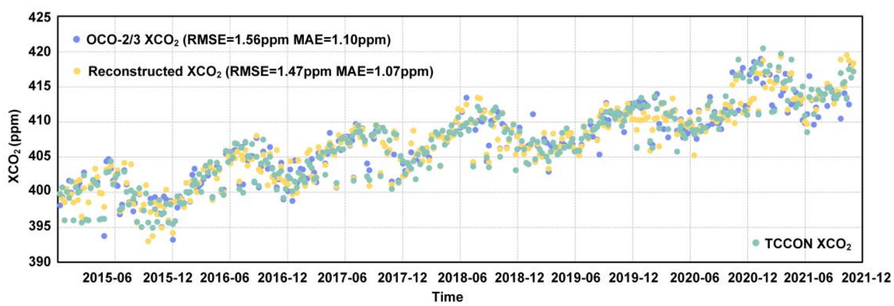

Figure 8. Comparison of the temporal variation of XCO_2 data from OCO-2/3 (blue dots), TCCON (green dots), and the reconstructed products (yellow dots).

https://doi.org/10.5194/essd-2024-315
Preprint. Discussion started: 25 October 2024

3.1.3 Product assessment with previous XCO_2 products

Fig. 9 shows the comparison between different XCO_2 products (i.e., original OCO XCO_2, CAMS-EGG4 GHGs data, and our reconstructed XCO_2) in four specific regions. The original OCO XCO_2 data were aggregated into 2°×2° latitude/longitude bins following Taylor et al. (2020). The CAMS-EGG4 GHGs data are a global reanalysis dataset at a spatial resolution of 0.75° released by the European Centre for Medium-range Weather Forecasts (Agustí-Panareda et al., 2023). The North America, Europe and part of north Africa, Asia and Oceania were chosen as examples. As shown in Fig. 9, the spatial coverage of CAMS-EGG4 GHGs data and our reconstructed XCO_2 is significantly increased compared to the original OCO XCO_2 data. However, the CAMS-EGG4 GHGs data is at a coarse spatial resolution and miss much of the detailed information on XCO_2 change. In comparison, our reconstructed seamless XCO_2 product can provide much more information on the global and regional spatial patterns of XCO_2. Due to the limited coverage, the original OCO XCO_2 data failed to capture the variation of XCO_2 in the Midwestern United States, northern part of the United Kingdom, and central China. In contrast, these regions are well represented in the reconstructed XCO_2 product. Furthermore, the reconstructed XCO_2 with a fine spatial resolution can offer a more accurate spatial distribution of carbon sources and sinks. For example, lower XCO_2 concentrations are clearly observed in the forests in eastern Canada and Papua New Guinea (Fig. c and l), indicating the great potential carbon sink of these areas. While the CAMS-EGG4 GHGs data cannot capture this change due to their coarse spatial resolutions. In general, reconstructed XCO_2 products with complete coverage and finer resolution provide valuable support for analyzing atmospheric CO_2 variation and accurate monitoring of carbon sources and sinks.

https://doi.org/10.5194/essd-2024-315
Preprint. Discussion started: 25 October 2024

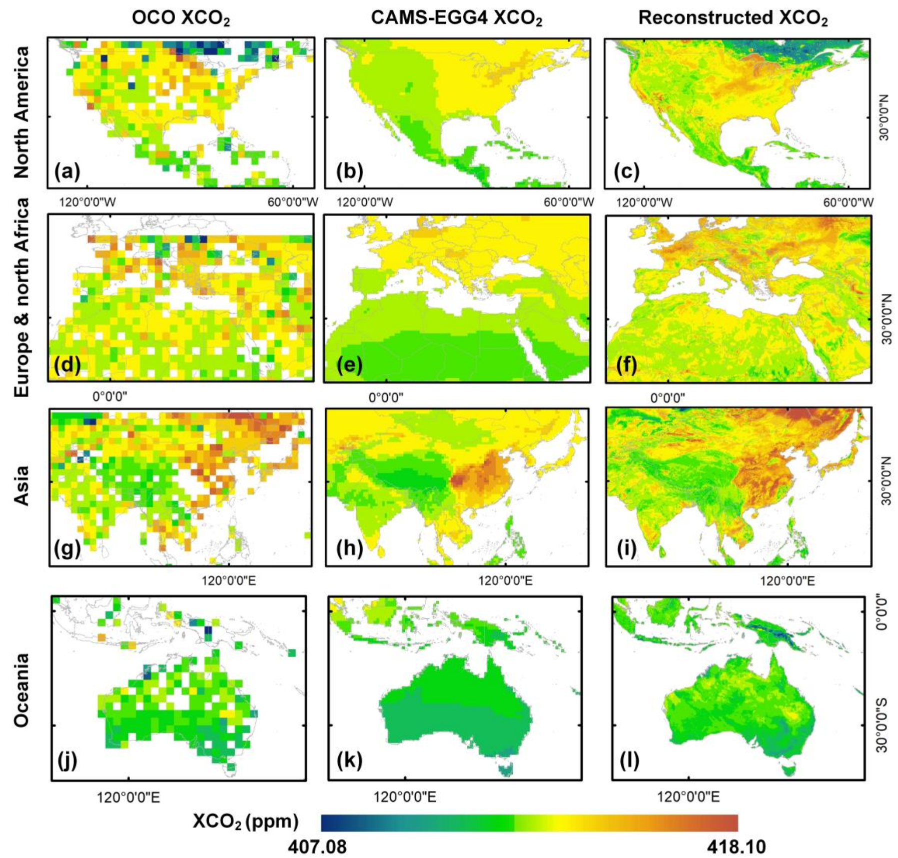

Figure 9. Comparison between the OCO observed XCO_2 data aggregated into 2°×2° latitude/longitude bins, the CAMS-EGG4 GHGs data, and our reconstructed XCO_2 data in four regions, using the products of December of 2020 as an example.

3.2 Spatiotemporal pattern of global XCO_2

The average XCO_2 concentration from 2015 to 2021 was 406.90 ± 0.80 ppm across the globe. The atmospheric CO_2 exhibited an apparent spatial variation, with higher concentrations typically observed in the Northern Hemisphere and lower concentrations in the Southern Hemisphere (Fig. 10a). The highest concentration of XCO_2 mainly occurs in the northern low-to-mid-latitudes (10°N-45°N), such as East Asia, southern Northern America, and the Middle East. More frequent human activities and carbon emissions contributed to higher atmospheric CO_2 concentrations in the Northern Hemisphere. In contrast, the lowest XCO_2 concentration was 404.02 ppm, occurring in the Southern Hemisphere where 81% of the area is ocean. The oceans act as a vital carbon sink and absorb most atmospheric CO_2. For the continent scale, the

XCO_2 concentrations showed a slight variation (±1 ppm) between different continents. The largest XCO_2 were mainly occurred in Asia and North America over years, while the lowest XCO_2 concentration all presented in Oceania (Table 4).

Fig. 10b presents the spatial distribution of the 7-year (2015-2021) XCO_2 trend over the globe. In terms of temporal trend, the atmospheric CO_2 exhibited a distinct increasing trend over time, with the mean growth rate of 2.32 ppm yr^{-1}. The large growth rate meanly occurs in the northern low latitudes (0°N-30°N), especially the Middle East and North Africa (growth rate over 2.5 ppm yr^{-1}). Globally, the XCO_2 increased by 14.16 ppm over seven years (Table 4), especially in 2021, with increased values of up to 3 ppm. This result is consistent with the Global Carbon Budget 2022 (Friedlingstein et al., 2022), which reported that the global average atmospheric CO_2 increased sharply in 2021 and reached 414.71 ppm.

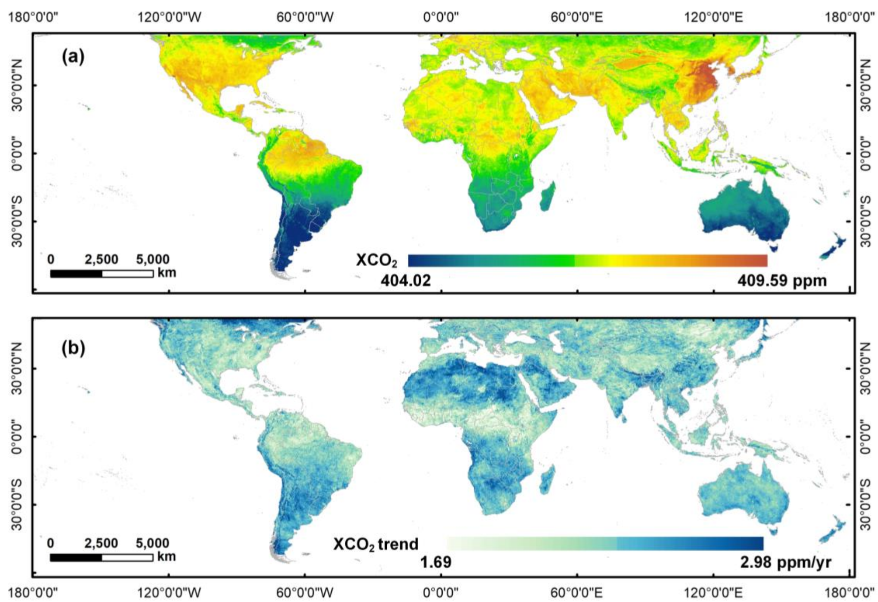

Figure 10. The global spatial distribution of (a) reconstructed annual mean XCO_2 concentration, and (b) its trend from 2015 to 2021 (ppm yr^{-1} denotes parts per million per year).

https://doi.org/10.5194/essd-2024-315
Preprint. Discussion started: 25 October 2024

Table 4. The reconstructed XCO_2 concentrations at different continents from 2015 to 2021.

Continents	XCO_2 concentrations (ppm)							
	2015	2016	2017	2018	2019	2020	2021	Increase
Africa	399.26	402.66	404.98	406.71	409.26	411.13	414.11	14.85
Asia	399.57	**403.03**	**405.80**	**407.37**	409.68	411.39	**414.38**	14.81
Europe	399.55	402.88	405.77	406.96	409.48	411.30	414.17	14.62
North America	**399.60**	402.95	405.76	407.32	**409.70**	**411.61**	414.28	14.68
South America	398.94	401.96	404.27	406.17	408.78	410.47	413.57	14.63
Oceania	398.03	401.04	403.31	405.53	408.13	409.82	412.55	14.52
Global	399.84	401.56	405.16	407.50	409.21	411.07	414.00	14.16

3.3 The distribution of XCO_2 anomaly

To better explore the dynamics of global carbon change, we further calculated the XCO_2 anomalies based on the full-coverage XCO_2 products and presented their global distributions from 2015 to 2021 (Fig. 11). The XCO_2 anomalies were calculated by the statistical filtering method, that is, subtracting the global median XCO_2 value from the global XCO_2 distribution (Hakkarainen et al., 2016). The spatial pattern of XCO_2 anomalies were relatively consistent over seven years with no significant variations. From the global perspective, high XCO_2 anomalies mainly occurred in the Northern Hemisphere. East Asia has the largest XCO_2 anomalies with values ranging from 2 to 3 ppm, such as the east part of China. The Middle East, North Africa and the southern part of Northern America also experienced high XCO_2 anomalies. Nevertheless, negative XCO_2 anomalies were also identified in the Northern Hemisphere, specifically in regions such as Tibet in China, eastern Canada, and southern Russia. Most negative XCO_2 anomalies were observed in the Southern Hemisphere, which behaves as a carbon sink. However, some positive XCO_2 anomalies are also observed in the tropical regions (e.g., Amazonia), which indicates the Amazonia has changed into a carbon source due to the deforestation and fire occurrence in recent years (Hubau et al., 2020; Gatti et al., 2021).

https://doi.org/10.5194/essd-2024-315
Preprint. Discussion started: 25 October 2024

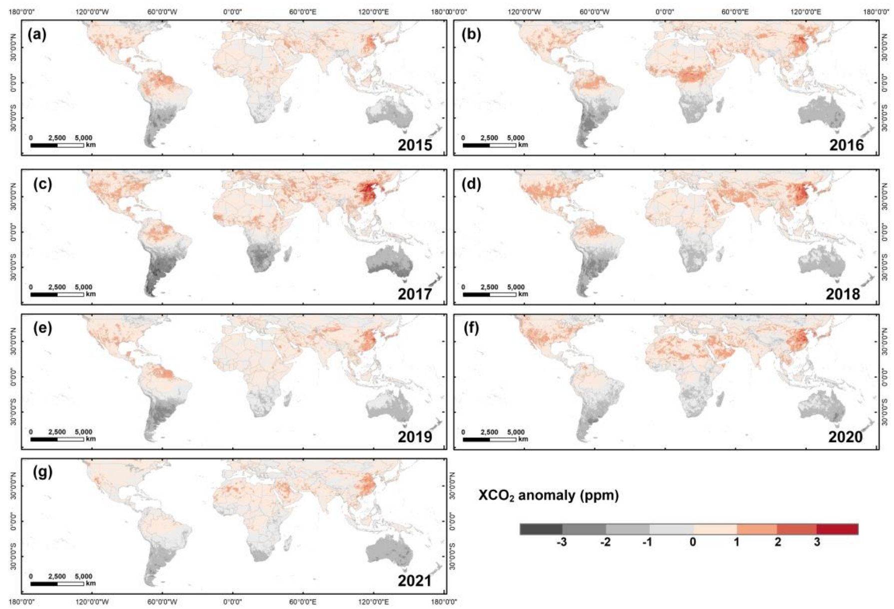

Figure 11. The global spatial distribution of annual XCO_2 anomaly from 2015 to 2021.

Fig. 12 illustrates the detailed spatial distribution of XCO_2 concentrations and anomalies over six regions with high XCO_2 retrievals in 2020. High concentrations of XCO_2 were typically associated with energy-intensive heavy industrial activities, such as Toa Oil Keihin Refinery Factory located in Kawasaki City, Japan (Fig. 12f), and the Shippingport Industrial Park in Pennsylvania, United States (Fig. 12a). Moreover, certain metropolitan transport hubs also exhibited elevated CO_2 anomalies attributable to dense populations and intensive activities. Examples included Shanghai Station in China (Fig.12e) and John F. Kennedy International Airport in New York, USA (Fig. 12b). Attention has also been drawn to natural sources of emissions. Driven by the significant impact of agricultural mechanization and agro-industrial activities on cropland (Lin and Xu, 2018), the XCO_2 anomalies also occurred in the agricultural areas northwestern Jiangsu, China (Fig. 12d). Additionally, we also observed the high XCO_2 anomalies in Amazonia forest in Colombia, which have been suffered from deforestation (Gatti et al., 2023). In conclusion, our products could successfully capture the XCO_2 anomalies from different sources over the globe.

https://doi.org/10.5194/essd-2024-315
Preprint. Discussion started: 25 October 2024

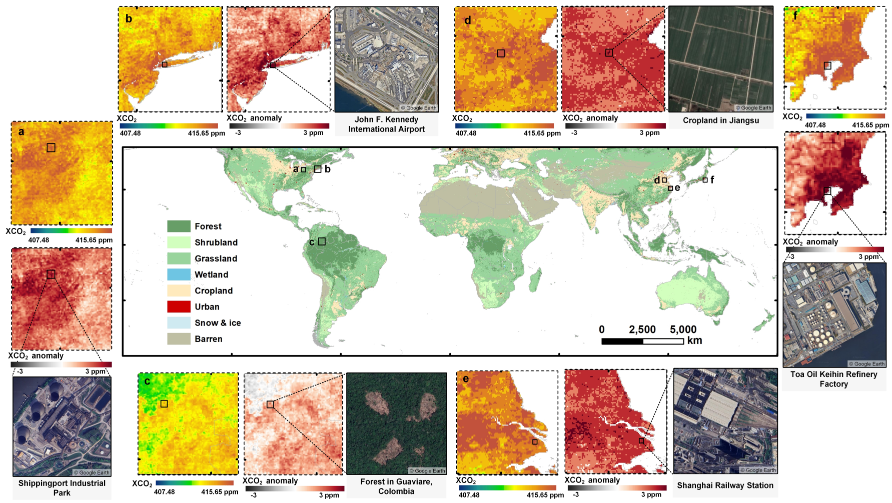

Figure 12. Examples of XCO_2 hotspots in six regions for 2020 detected using the reconstructed products. The subplots present the spatial distribution of XCO_2 concentrations, anomalies (the red panels), and the emission sources (the true color images from © Google Earth), respectively. The global map in the middle presents the land use and land cover types over the globe.

4. Discussion

In this study, we utilized deep learning and multi-source satellite data (i.e., OCO2/3, MODIS, VIIRS and TROPOMI) to reconstruct global XCO_2 products at a spatial resolution of 0.05°×0.05°. Though our products achieved full spatial coverage and high accuracy, there are still several limitations need further improvement. In terms of sensors, OCO-2 and OCO-3 data provide different spatiotemporal coverages. Analyzing OCO-2 and OCO-3 data simultaneously may introduce several uncertainties due to these differences. However, OCO-3 has a similar sensor and inherits the retrieval algorithms of OCO-2. According to Taylor et al. (2023), the mean differences between OCO-3 and OCO-2 are around 0.2 ppm over land. Therefore, we suppose that the discrepancies between their datasets are minimal, and the combined analysis of data from these two satellites will have a negligible impact on our results.

Moreover, despite OCO is considered to be one of the most accurate carbon satellite datasets to date, it still encounters some retrieval errors due to the influence of retrieval methods and meteorology conditions, which may be introduced by using the data as a target for XCO_2 reconstruction. However, the validation results against TCCON suggested that the RMSEs of the two OCO XCO_2 datasets are both less than

https://doi.org/10.5194/essd-2024-315
Preprint. Discussion started: 25 October 2024

1 ppm, which is sufficient for monitoring changes in atmospheric CO_2 (Taylor et al., 2023).

Additionally, prediction uncertainty may also arise from the model and covariates used (Chen et al., 2022). While our deep learning model achieved high accuracy in general, its performance in the Southern Hemisphere could be further improved. This is attributed to the distribution of data features and the complex non-linear relationship between XCO_2 and the environmental covariates. Selecting more relevant environmental factors may help mitigate these issues and enhance model performance in this region.

5. Data availability

The XCO_2 dataset produced in this paper is available at https://doi.org/10.5281/zenodo.12706142 (Wang et al., 2024). It includes monthly global XCO_2 data at 0.05° resolution, covering the period from December 2014 to December 2021. The dataset is archived in netCDF4 format, with units in parts per million (ppm).

6. Conclusion

The launch of carbon satellites offers a significant advancement for CO_2 monitoring. However, their limited spatial coverage restricts the effectiveness of XCO_2 data. To address this issue, we reconstructed a global full-coverage XCO_2 product at a fine spatial resolution using multi-component satellite data. The advanced deep learning method was adopted to model time-series XCO_2 and incorporate terrestrial flux, anthropogenic flux and climatic impacts into the parameterization process. Our reconstructed XCO_2 products showed a strong agreement with TCCON XCO_2, with R^2, RMSE, and MAE values of 0.92, 1.54 ppm, and 1.09 ppm, respectively. The products provided accurate information on the global and regional spatial pattern of XCO_2. The global XCO_2 exhibited a distinct increasing trend over time, reaching 414.00 ppm in 2021. Higher XCO_2 concentrations were primarily observed in the northern low-to-mid-latitudes (10°N-45°N) such as Asia and North America. Utilizing the reconstructed products, we further detected XCO_2 anomalies globally and identified intensive carbon emission sources across different land use types. Our study presents a viable method for global-scale, high-resolution XCO_2 mapping based on carbon satellites and

https://doi.org/10.5194/essd-2024-315
Preprint. Discussion started: 25 October 2024

demonstrates the feasibility of applying this methodology to explore global and regional carbon dynamics.

Acknowledgements

The authors would like to express their gratitude to the NASA Goddard Earth Science Data and Information Services Center for providing the OCO-2/3 XCO_2 products (https://disc.gsfc.nasa.gov/), the NASA Land Processes Distributed Active Archive Center (LP DAAC) for providing MODIS data. Our gratitude also goes to the Earth Observation Group (EOG) of the Colorado School of Mines for supplying the NPP-VIIRS NTL products, the European Space Agency (ESA) for providing the TROPOMI data, the Copernicus Climate Data Store for providing the ERA5 reanalysis data and CAMS-EGG4 XCO_2 data, and the Total Carbon Column Observing Network for their dedication in providing the in situ XCO_2 observations.

Author contributions

ZW developed the overall workflow, processed the data and wrote the manuscript. CZ and BH revised the manuscript. KS, YS, and XC compiled the data. SC conceptualized and revised the manuscript. PA and QZ supervised this study. All the authors contributed to the study.

Competing interests

The contact author has declared that none of the authors has any competing interests.

Financial support

This work was supported by the Key R&D Program of Zhejiang (2022C03078) and National Natural Science Foundation of China (NSFC) (32241036).

References

Agustí-Panareda, A., Barré, J., Massart, S., Inness, A., Aben, I., Ades, M., Baier, B.C., Balsamo, G., Borsdorff, T., Bousserez, N., Boussetta, S., Buchwitz, M., Cantarello, L., Crevoisier, C., Engelen, R., Eskes, H., Flemming, J., Garrigues, S., Hasekamp, O., Huijnen, V., Jones, L., Kipling, Z., Langerock, B., McNorton, J., Meilhac, N., Noël, S., Parrington, M., Peuch, V.-H., Ramonet, M., Razinger, M., Reuter, M., Ribas, R., Suttie, M., Sweeney, C., Tarniewicz, J., Wu, L., 2023. Technical note: The CAMS greenhouse gas reanalysis from 2003 to 2020. Atmos. Chem. Phys. 23, 3829–3859. https://doi.org/10.5194/acp-23-3829-2023

Bacastow, R.B., Keeling, C.D., Whorf, T.P., 1985. Seasonal amplitude increase in atmospheric CO_2 concentration at Mauna Loa, Hawaii, 1959–1982. J. Geophys.

https://doi.org/10.5194/essd-2024-315
Preprint. Discussion started: 25 October 2024

Res. Atmos. 90, 10529–10540. https://doi.org/10.1029/JD090iD06p10529

Bahdanau, D., Cho, K., Bengio, Y., 2016. Neural Machine Translation by Jointly Learning to Align and Translate. https://doi.org/10.48550/arXiv.1409.0473

Beer, C., Reichstein, M., Tomelleri, E., Ciais, P., Jung, M., Carvalhais, N., Rödenbeck, C., Arain, M.A., Baldocchi, D., Bonan, G.B., Bondeau, A., Cescatti, A., Lasslop, G., Lindroth, A., Lomas, M., Luyssaert, S., Margolis, H., Oleson, K.W., Roupsard, O., Veenendaal, E., Viovy, N., Williams, C., Woodward, F.I., Papale, D., 2010. Terrestrial Gross Carbon Dioxide Uptake: Global Distribution and Covariation with Climate. Science 329, 834–838. https://doi.org/10.1126/science.1184984

Bovensmann, H., Burrows, J.P., Buchwitz, M., Frerick, J., Noël, S., Rozanov, V.V., Chance, K.V., Goede, A.P.H., 1999. SCIAMACHY: Mission Objectives and Measurement Modes. J. Atmos. Sci. 56, 127–150. https://doi.org/10.1175/1520-0469(1999)056<0127:SMOAMM>2.0.CO;2

Buchwitz, M., Reuter, M., Schneising, O., Boesch, H., Guerlet, S., Dils, B., Aben, I., Armante, R., Bergamaschi, P., Blumenstock, T., Bovensmann, H., Brunner, D., Buchmann, B., Burrows, J.P., Butz, A., Chédin, A., Chevallier, F., Crevoisier, C.D., Deutscher, N.M., Frankenberg, C., Hase, F., Hasekamp, O.P., Heymann, J., Kaminski, T., Laeng, A., Lichtenberg, G., De Mazière, M., Noël, S., Notholt, J., Orphal, J., Popp, C., Parker, R., Scholze, M., Sussmann, R., Stiller, G.P., Warneke, T., Zehner, C., Bril, A., Crisp, D., Griffith, D.W.T., Kuze, A., O'Dell, C., Oshchepkov, S., Sherlock, V., Suto, H., Wennberg, P., Wunch, D., Yokota, T., Yoshida, Y., 2015. The Greenhouse Gas Climate Change Initiative (GHG-CCI): Comparison and quality assessment of near-surface-sensitive satellite-derived CO2 and CH4 global data sets. Remote Sens. Environ. 162, 344–362. https://doi.org/10.1016/j.rse.2013.04.024

Butz, A., Guerlet, S., Hasekamp, O., Schepers, D., Galli, A., Aben, I., Frankenberg, C., Hartmann, J.-M., Tran, H., Kuze, A., Keppel-Aleks, G., Toon, G., Wunch, D., Wennberg, P., Deutscher, N., Griffith, D., Macatangay, R., Messerschmidt, J., Notholt, J., Warneke, T., 2011. Toward accurate CO2 and CH4 observations from GOSAT. Geophys. Res. Lett. 38. https://doi.org/10.1029/2011GL047888

Canadell, J.G., Le Quéré, C., Raupach, M.R., Field, C.B., Buitenhuis, E.T., Ciais, P., Conway, T.J., Gillett, N.P., Houghton, R.A., Marland, G., 2007. Contributions to accelerating atmospheric CO_2 growth from economic activity, carbon intensity, and efficiency of natural sinks. Proc. Natl. Acad. Sci. USA 104, 18866–18870. https://doi.org/10.1073/pnas.0702737104

Chen, Y., Feng, X., Tian, H., Wu, X., Gao, Z., Feng, Y., Piao, S., Lv, N., Pan, N., Fu, B., 2021. Accelerated increase in vegetation carbon sequestration in China after 2010: A turning point resulting from climate and human interaction. Global Change Biology 27, 5848–5864. https://doi.org/10.1111/gcb.15854

Chen, Z., Huntzinger, D.N., Liu, J., Piao, S., Wang, X., Sitch, S., Friedlingstein, P., Anthoni, P., Arneth, A., Bastrikov, V., Goll, D.S., Haverd, V., Jain, A.K., Joetzjer, E., Kato, E., Lienert, S., Lombardozzi, D.L., McGuire, P.C., Melton, J.R., Nabel, J.E.M.S., Pongratz, J., Poulter, B., Tian, H., Wiltshire, A.J., Zaehle, S., Miller, S.M., 2021. Five years of variability in the global carbon cycle: comparing an estimate from the Orbiting Carbon Observatory-2 and process-based models. Environ. Res. Lett. 16, 054041. https://doi.org/10.1088/1748-9326/abfac1

Chen, S., Arrouays, D., Mulder, V.L., Poggio, L., Minasny, B., Roudier, P., Libohova, Z., Lagacherie, P., Shi, Z., Hannam, J. and Meersmans, J., 2022. Digital mapping of GlobalSoilMap soil properties at a broad scale: A review. Geoderma 409, 115567. https://doi.org/10.1016/j.geoderma.2021.115567

Chen, S., Wang, W., Xu, W., Wang, Yang, Wan, H., Chen, D., Tang, Z., Tang, X., Zhou, G., Xie, Z., Zhou, D., Shangguan, Z., Huang, J., He, J.-S., Wang, Yanfen, Sheng, J., Tang, L., Li, X., Dong, M., Wu, Y., Wang, Q., Wang, Z., Wu, J., Chapin, F.S., Bai, Y., 2018. Plant diversity enhances productivity and soil carbon storage. Proc. Natl. Acad. Sci. 115, 4027–4032. https://doi.org/10.1073/pnas.1700298114

Connor, B.J., Boesch, H., Toon, G., Sen, B., Miller, C., Crisp, D., 2008. Orbiting Carbon Observatory: Inverse method and prospective error analysis. J. Geophys. Res.-Atmos. 113. https://doi.org/10.1029/2006JD008336

Crisp, D., Atlas, R.M., Breon, F.-M., Brown, L.R., Burrows, J.P., Ciais, P., Connor, B.J., Doney, S.C., Fung, I.Y., Jacob, D.J., Miller, C.E., O'Brien, D., Pawson, S., Randerson, J.T., Rayner, P., Salawitch, R.J., Sander, S.P., Sen, B., Stephens, G.L., Tans, P.P., Toon, G.C., Wennberg, P.O., Wofsy, S.C., Yung, Y.L., Kuang, Z., Chudasama, B., Sprague, G., Weiss, B., Pollock, R., Kenyon, D., Schroll, S., 2004. The Orbiting Carbon Observatory (OCO) mission. Adv. Space Res. 34, 700–709. https://doi.org/10.1016/j.asr.2003.08.062

Crisp, D., Pollock, H.R., Rosenberg, R., Chapsky, L., Lee, R.A.M., Oyafuso, F.A., Frankenberg, C., O'Dell, C.W., Bruegge, C.J., Doran, G.B., Eldering, A., Fisher, B.M., Fu, D., Gunson, M.R., Mandrake, L., Osterman, G.B., Schwandner, F.M., Sun, K., Taylor, T.E., Wennberg, P.O., Wunch, D., 2017. The on-orbit performance of the Orbiting Carbon Observatory-2 (OCO-2) instrument and its radiometrically calibrated products. Atmos. Meas. Tech. 10, 59–81. https://doi.org/10.5194/amt-10-59-2017

Crisp, D., O'Dell, C., Eldering, A., Fisher, B., Oyafuso, F., Payne, V., Drouin, B., Toon, G., Laughner, J., Somkuti, P., McGarragh, G., Merrelli, A., Nelson, R., Gunson, M., Frankenberg, C., Osterman, G., Boesch, H., Brown, L., Castano, R., Christi, M., Connor, B., McDuffie, J., Miller, C., Natraj, V., O'Brien, D., Polonsky, I., Smyth, M., Thompson, D., and Granat, R., 2020. Orbiting Carbon Observatory-2 & 3 Level 2 Full Physics Retrieval Algorithm Theoretical Basis, v10, Tech. rep., Jet Propulsion Laboratory, https://docserver.gesdisc.eosdis.nasa.gov/public/project/OCO/OCO_L2_ATBD.pdf (last access: 15 June 2023)

Deng, F., Jones, D.B.A., O'Dell, C.W., Nassar, R., Parazoo, N.C., 2016. Combining GOSAT XCO_2 observations over land and ocean to improve regional CO_2 flux estimates. J. Geophys. Res. Atmos. 121, 1896–1913. https://doi.org/10.1002/2015JD024157

Duren, R.M., Miller, C.E., 2012. Measuring the carbon emissions of megacities. Nature Clim. Change 2, 560–562. https://doi.org/10.1038/nclimate1629

Eldering, A., Taylor, T.E., O'Dell, C.W., Pavlick, R., 2019. The OCO-3 mission: measurement objectives and expected performance based on 1 year of simulated data. Atmos. Meas. Tech. 12, 2341–2370. https://doi.org/10.5194/amt-12-2341-2019

Eldering, A., Wennberg, P.O., Crisp, D., Schimel, D.S., Gunson, M.R., Chatterjee, A., Liu, J., Schwandner, F.M., Sun, Y., O'Dell, C.W., Frankenberg, C., Taylor, T., Fisher, B., Osterman, G.B., Wunch, D., Hakkarainen, J., Tamminen, J., Weir, B., 2017. The Orbiting Carbon Observatory-2 early science investigations of regional carbon dioxide fluxes. Science 358, eaam5745. https://doi.org/10.1126/science.aam5745

Feldman, A.F., Zhang, Z., Yoshida, Y., Chatterjee, A., Poulter, B., 2023. Using Orbiting Carbon Observatory-2 (OCO-2) column CO_2 retrievals to rapidly detect and estimate biospheric surface carbon flux anomalies. Atmos. Chem. Phys. 23, 1545–

1563. https://doi.org/10.5194/acp-23-1545-2023

Fernández-Martínez, M., Peñuelas, J., Chevallier, F., Ciais, P., Obersteiner, M., Rödenbeck, C., Sardans, J., Vicca, S., Yang, H., Sitch, S., Friedlingstein, P., Arora, V.K., Goll, D.S., Jain, A.K., Lombardozzi, D.L., McGuire, P.C., Janssens, I.A., 2023. Diagnosing destabilization risk in global land carbon sinks. Nature 615, 848–853. https://doi.org/10.1038/s41586-023-05725-1

Fernández-Martínez, M., Sardans, J., Chevallier, F., Ciais, P., Obersteiner, M., Vicca, S., Canadell, J.G., Bastos, A., Friedlingstein, P., Sitch, S., Piao, S.L., Janssens, I.A., Peñuelas, J., 2019. Global trends in carbon sinks and their relationships with CO2 and temperature. Nature Clim. Change 9, 73–79. https://doi.org/10.1038/s41558-018-0367-7

Forkel, M., Carvalhais, N., Rödenbeck, C., Keeling, R., Heimann, M., Thonicke, K., Zaehle, S., Reichstein, M., 2016. Enhanced seasonal CO_2 exchange caused by amplified plant productivity in northern ecosystems. Science 351, 696–699. https://doi.org/10.1126/science.aac4971

Friedlingstein, P., O'Sullivan, M., Jones, M.W., Andrew, R.M., Gregor, L., Hauck, J., Le Quéré, C., Luijkx, I.T., Olsen, A., Peters, G.P., Peters, W., Pongratz, J., Schwingshackl, C., Sitch, S., Canadell, J.G., Ciais, P., Jackson, R.B., Alin, S.R., Alkama, R., Arneth, A., Arora, V.K., Bates, N.R., Becker, M., Bellouin, N., Bittig, H.C., Bopp, L., Chevallier, F., Chini, L.P., Cronin, M., Evans, W., Falk, S., Feely, R.A., Gasser, T., Gehlen, M., Gkritzalis, T., Gloege, L., Grassi, G., Gruber, N., Gürses, Ö., Harris, I., Hefner, M., Houghton, R.A., Hurtt, G.C., Iida, Y., Ilyina, T., Jain, A.K., Jersild, A., Kadono, K., Kato, E., Kennedy, D., Klein Goldewijk, K., Knauer, J., Korsbakken, J.I., Landschützer, P., Lefèvre, N., Lindsay, K., Liu, J., Liu, Z., Marland, G., Mayot, N., McGrath, M.J., Metzl, N., Monacci, N.M., Munro, D.R., Nakaoka, S.-I., Niwa, Y., O'Brien, K., Ono, T., Palmer, P.I., Pan, N., Pierrot, D., Pocock, K., Poulter, B., Resplandy, L., Robertson, E., Rödenbeck, C., Rodriguez, C., Rosan, T.M., Schwinger, J., Séférian, R., Shutler, J.D., Skjelvan, I., Steinhoff, T., Sun, Q., Sutton, A.J., Sweeney, C., Takao, S., Tanhua, T., Tans, P.P., Tian, X., Tian, H., Tilbrook, B., Tsujino, H., Tubiello, F., van der Werf, G.R., Walker, A.P., Wanninkhof, R., Whitehead, C., Willstrand Wranne, A., Wright, R., Yuan, W., Yue, C., Yue, X., Zaehle, S., Zeng, J., Zheng, B., 2022. Global Carbon Budget 2022. Earth Syst. Sci. Data 14, 4811–4900. https://doi.org/10.5194/essd-14-4811-2022

Friedlingstein, P., Houghton, R.A., Marland, G., Hackler, J., Boden, T.A., Conway, T.J., Canadell, J.G., Raupach, M.R., Ciais, P., Le Quéré, C., 2010. Update on CO_2 emissions. Nature Geosci 3, 811–812. https://doi.org/10.1038/ngeo1022

Friedman, J.H., 2001. Greedy Function Approximation: A Gradient Boosting Machine. The Annals of Statistics 29, 1189–1232.

Gatti, L.V., Basso, L.S., Miller, J.B., Gloor, M., Gatti Domingues, L., Cassol, H.L.G., Tejada, G., Aragão, L.E.O.C., Nobre, C., Peters, W., Marani, L., Arai, E., Sanches, A.H., Corrêa, S.M., Anderson, L., Von Randow, C., Correia, C.S.C., Crispim, S.P., Neves, R.A.L., 2021. Amazonia as a carbon source linked to deforestation and climate change. Nature 595, 388–393. https://doi.org/10.1038/s41586-021-03629-6

Gatti, L.V., Cunha, C.L., Marani, L., Cassol, H.L.G., Messias, C.G., Arai, E., Denning, A.S., Soler, L.S., Almeida, C., Setzer, A., Domingues, L.G., Basso, L.S., Miller, J.B., Gloor, M., Correia, C.S.C., Tejada, G., Neves, R.A.L., Rajao, R., Nunes, F., Filho, B.S.S., Schmitt, J., Nobre, C., Corrêa, S.M., Sanches, A.H., Aragão, L.E.O.C., Anderson, L., Von Randow, C., Crispim, S.P., Silva, F.M., Machado,

https://doi.org/10.5194/essd-2024-315
Preprint. Discussion started: 25 October 2024

G.B.M., 2023. Increased Amazon carbon emissions mainly from decline in law enforcement. Nature 621, 318–323. https://doi.org/10.1038/s41586-023-06390-0

Gentine, P., Green, J.K., Guérin, M., Humphrey, V., Seneviratne, S.I., Zhang, Y., Zhou, S., 2019. Coupling between the terrestrial carbon and water cycles-a review. Environ. Res. Lett. 14, 083003. https://doi.org/10.1088/1748-9326/ab22d6

Graven, H.D., Keeling, R.F., Piper, S.C., Patra, P.K., Stephens, B.B., Wofsy, S.C., Welp, L.R., Sweeney, C., Tans, P.P., Kelley, J.J., Daube, B.C., Kort, E.A., Santoni, G.W., Bent, J.D., 2013. Enhanced Seasonal Exchange of CO_2 by Northern Ecosystems Since 1960. Science 341, 1085–1089. https://doi.org/10.1126/science.1239207

Graves, A., Fernández, S., & Schmidhuber, J. 2005. Bidirectional LSTM networks for improved phoneme classification and recognition. In Artificial Neural Networks: Formal Models and Their Applications–ICANN 2005: 15th International Conference, Warsaw, Poland, September 11-15, 2005. Proceedings, Part II 15 (pp. 799-804). Springer Berlin Heidelberg.

Green, J.K., Seneviratne, S.I., Berg, A.M., Findell, K.L., Hagemann, S., Lawrence, D.M., Gentine, P., 2019. Large influence of soil moisture on long-term terrestrial carbon uptake. Nature 565, 476–479. https://doi.org/10.1038/s41586-018-0848-x

Hakkarainen, J., Ialongo, I., Tamminen, J., 2016. Direct space-based observations of anthropogenic CO_2 emission areas from OCO-2. Geophys. Res. Lett. 43, 11,400-11,406. https://doi.org/10.1002/2016GL070885

Hammerling, D.M., Michalak, A.M., Kawa, S.R., 2012. Mapping of CO_2 at high spatiotemporal resolution using satellite observations: Global distributions from OCO-2. J. Geophys. Res. Atmos. 117. https://doi.org/10.1029/2011JD017015

Harris, N.L., Gibbs, D.A., Baccini, A., Birdsey, R.A., de Bruin, S., Farina, M., Fatoyinbo, L., Hansen, M.C., Herold, M., Houghton, R.A., Potapov, P.V., Suarez, D.R., Roman-Cuesta, R.M., Saatchi, S.S., Slay, C.M., Turubanova, S.A., Tyukavina, A., 2021. Global maps of twenty-first century forest carbon fluxes. Nat. Clim. Chang. 11, 234–240. https://doi.org/10.1038/s41558-020-00976-6

He, C., Ji, M., Li, T., Liu, X., Tang, D., Zhang, S., Luo, Y., Grieneisen, M.L., Zhou, Z., Zhan, Y., 2022. Deriving Full-Coverage and Fine-Scale XCO_2 Across China Based on OCO-2 Satellite Retrievals and CarbonTracker Output. Geophys. Res. Lett. 49, e2022GL098435. https://doi.org/10.1029/2022GL098435

He, Z., Lei, L., Zhang, Y., Sheng, M., Wu, C., Li, L., Zeng, Z.-C., Welp, L.R., 2020. Spatio-Temporal Mapping of Multi-Satellite Observed Column Atmospheric CO_2 Using Precision-Weighted Kriging Method. Remote Sens. 12, 576. https://doi.org/10.3390/rs12030576

Heinze, C., Meyer, S., Goris, N., Anderson, L., Steinfeldt, R., Chang, N., Le Quéré, C., Bakker, D.C.E., 2015. The ocean carbon sink - impacts, vulnerabilities and challenges. Earth Syst. Dynam. 6, 327–358. https://doi.org/10.5194/esd-6-327-2015

Hersbach, H., Bell, B., Berrisford, P., Hirahara, S., Horányi, A., Muñoz-Sabater, J., Nicolas, J., Peubey, C., Radu, R., Schepers, D., Simmons, A., Soci, C., Abdalla, S., Abellan, X., Balsamo, G., Bechtold, P., Biavati, G., Bidlot, J., Bonavita, M., De Chiara, G., Dahlgren, P., Dee, D., Diamantakis, M., Dragani, R., Flemming, J., Forbes, R., Fuentes, M., Geer, A., Haimberger, L., Healy, S., Hogan, R.J., Hólm, E., Janisková, M., Keeley, S., Laloyaux, P., Lopez, P., Lupu, C., Radnoti, G., de Rosnay, P., Rozum, I., Vamborg, F., Villaume, S., Thépaut, J.-N., 2020. The ERA5 global reanalysis. Q. J. R. Meteorol. Soc. 146, 1999–2049. https://doi.org/10.1002/qj.3803

Hochreiter, S., Schmidhuber, J., 1997. Long Short-Term Memory. Neural Comput. 9, 1735–1780. https://doi.org/10.1162/neco.1997.9.8.1735

Hubau, W., Lewis, S.L., Phillips, O.L., Affum-Baffoe, K., Beeckman, H., Cuní-Sanchez, A., Daniels, A.K., Ewango, C.E.N., Fauset, S., Mukinzi, J.M., Sheil, D., Sonké, B., Sullivan, M.J.P., Sunderland, T.C.H., Taedoumg, H., Thomas, S.C., White, L.J.T., Abernethy, K.A., Adu-Bredu, S., Amani, C.A., Baker, T.R., Banin, L.F., Baya, F., Begne, S.K., Bennett, A.C., Benedet, F., Bitariho, R., Bocko, Y.E., Boeckx, P., Boundja, P., Brienen, R.J.W., Brncic, T., Chezeaux, E., Chuyong, G.B., Clark, C.J., Collins, M., Comiskey, J.A., Coomes, D.A., Dargie, G.C., de Haulleville, T., Kamdem, M.N.D., Doucet, J.-L., Esquivel-Muelbert, A., Feldpausch, T.R., Fofanah, A., Foli, E.G., Gilpin, M., Gloor, E., Gonmadje, C., Gourlet-Fleury, S., Hall, J.S., Hamilton, A.C., Harris, D.J., Hart, T.B., Hockemba, M.B.N., Hladik, A., Ifo, S.A., Jeffery, K.J., Jucker, T., Yakusu, E.K., Kearsley, E., Kenfack, D., Koch, A., Leal, M.E., Levesley, A., Lindsell, J.A., Lisingo, J., Lopez-Gonzalez, G., Lovett, J.C., Makana, J.-R., Malhi, Y., Marshall, A.R., Martin, J., Martin, E.H., Mbayu, F.M., Medjibe, V.P., Mihindou, V., Mitchard, E.T.A., Moore, S., Munishi, P.K.T., Bengone, N.N., Ojo, L., Ondo, F.E., Peh, K.S.-H., Pickavance, G.C., Poulsen, A.D., Poulsen, J.R., Qie, L., Reitsma, J., Rovero, F., Swaine, M.D., Talbot, J., Taplin, J., Taylor, D.M., Thomas, D.W., Toirambe, B., Mukendi, J.T., Tuagben, D., Umunay, P.M., van der Heijden, G.M.F., Verbeeck, H., Vleminckx, J., Willcock, S., Wöll, H., Woods, J.T., Zemagho, L., 2020. Asynchronous carbon sink saturation in African and Amazonian tropical forests. Nature 579, 80–87. https://doi.org/10.1038/s41586-020-2035-0

IPCC, 2023: Climate Change 2023: Synthesis Report. Contribution of Working Groups I, II and III to the Sixth Assessment Report of the Intergovernmental Panel on Climate Change [Core Writing Team, H. Lee and J. Romero (eds.)]. IPCC, Geneva, Switzerland, pp. 35-115, doi: 10.59327/IPCC/AR6-9789291691647

Inoue, M., Morino, I., Uchino, O., Miyamoto, Y., Yoshida, Y., Yokota, T., Machida, T., Sawa, Y., Matsueda, H., Sweeney, C., Tans, P.P., Andrews, A.E., Biraud, S.C., Tanaka, T., Kawakami, S., Patra, P.K., 2013. Validation of XCO2 derived from SWIR spectra of GOSAT TANSO-FTS with aircraft measurement data. Atmos. Chem. Phys. 13, 9771–9788. https://doi.org/10.5194/acp-13-9771-2013

Janardanan, R., Maksyutov, S., Oda, T., Saito, M., Kaiser, J.W., Ganshin, A., Stohl, A., Matsunaga, T., Yoshida, Y., Yokota, T., 2016. Comparing GOSAT observations of localized CO_2 enhancements by large emitters with inventory-based estimates. Geophys. Res. Lett. 43, 3486–3493. https://doi.org/10.1002/2016GL067843

Kaminski, T., Scholze, M., Vossbeck, M., Knorr, W., Buchwitz, M., Reuter, M., 2017. Constraining a terrestrial biosphere model with remotely sensed atmospheric carbon dioxide. Remote Sens. Environ. 203, 109–124. https://doi.org/10.1016/j.rse.2017.08.017

Kemp, L., Xu, C., Depledge, J., Ebi, K.L., Gibbins, G., Kohler, T.A., Rockström, J., Scheffer, M., Schellnhuber, H.J., Steffen, W., Lenton, T.M., 2022. Climate Endgame: Exploring catastrophic climate change scenarios. Proc. Natl. Acad. Sci. 119, e2108146119. https://doi.org/10.1073/pnas.2108146119

Kiel, M., Eldering, A., Roten, D.D., Lin, J.C., Feng, S., Lei, R., Lauvaux, T., Oda, T., Roehl, C.M., Blavier, J.-F., Iraci, L.T., 2021. Urban-focused satellite CO_2 observations from the Orbiting Carbon Observatory-3: A first look at the Los Angeles megacity. Remote Sens. Environ. 258, 112314. https://doi.org/10.1016/j.rse.2021.112314

Kiel, M., O'Dell, C.W., Fisher, B., Eldering, A., Nassar, R., MacDonald, C.G., Wennberg, P.O., 2019. How bias correction goes wrong: measurement of X_{CO2}

affected by erroneous surface pressure estimates. Atmos. Meas. Tech. 12, 2241–2259. https://doi.org/10.5194/amt-12-2241-2019

Labzovskii, L.D., Jeong, S.-J., Parazoo, N.C., 2019. Working towards confident spaceborne monitoring of carbon emissions from cities using Orbiting Carbon Observatory-2. Remote Sens. Environ. 233, 111359. https://doi.org/10.1016/j.rse.2019.111359

Lei, R., Feng, S., Danjou, A., Broquet, G., Wu, D., Lin, J.C., O'Dell, C.W., Lauvaux, T., 2021. Fossil fuel CO_2 emissions over metropolitan areas from space: A multi-model analysis of OCO-2 data over Lahore, Pakistan. Remote Sens. Environ. 264, 112625. https://doi.org/10.1016/j.rse.2021.112625

Lin, B., Xu, B., 2018. Factors affecting CO_2 emissions in China's agriculture sector: A quantile regression. Renewable and Sustainable Energy Reviews 94, 15–27. https://doi.org/10.1016/j.rser.2018.05.065

Liu, J., Bowman, K.W., Schimel, D.S., Parazoo, N.C., Jiang, Z., Lee, M., Bloom, A.A., Wunch, D., Frankenberg, C., Sun, Y., O'Dell, C.W., Gurney, K.R., Menemenlis, D., Gierach, M., Crisp, D., Eldering, A., 2017. Contrasting carbon cycle responses of the tropical continents to the 2015–2016 El Niño. Science 358, eaam5690. https://doi.org/10.1126/science.aam5690

Lundberg, S.M., Erion, G., Chen, H., DeGrave, A., Prutkin, J.M., Nair, B., Katz, R., Himmelfarb, J., Bansal, N., Lee, S.-I., 2020. From local explanations to global understanding with explainable AI for trees. Nat. Mach. Intell. 2, 56–67. https://doi.org/10.1038/s42256-019-0138-9

Lundberg, S.M., Lee, S.-I., 2017. A unified approach to interpreting model predictions, in: Proceedings of the 31st International Conference on Neural Information Processing Systems, NIPS'17. Curran Associates Inc., Red Hook, NY, USA, pp. 4768–4777.

Luong, M.-T., Pham, H., Manning, C.D., 2015. Effective Approaches to Attention-based Neural Machine Translation. CoRR abs/1508.04025.

Matthias Forkel et al., 2016. Enhanced seasonal CO_2 exchange caused by amplified plant productivity in northern ecosystems. Science 351, 696-699(2016). DOI:10.1126/science.aac4971

Nassar, R., Mastrogiacomo, J.-P., Bateman-Hemphill, W., McCracken, C., MacDonald, C.G., Hill, T., O'Dell, C.W., Kiel, M., Crisp, D., 2021. Advances in quantifying power plant CO_2 emissions with OCO-2. Remote Sens. Environ. 264, 112579. https://doi.org/10.1016/j.rse.2021.112579

Oda, T., Maksyutov, S., Andres, R.J., 2018. The Open-source Data Inventory for Anthropogenic CO_2, version 2016 (ODIAC2016): a global monthly fossil fuel CO_2 gridded emissions data product for tracer transport simulations and surface flux inversions. Earth Syst. Sci. Data 10, 87–107. https://doi.org/10.5194/essd-10-87-2018

O'Dell, C.W., Eldering, A., Wennberg, P.O., Crisp, D., Gunson, M.R., Fisher, B., Frankenberg, C., Kiel, M., Lindqvist, H., Mandrake, L., Merrelli, A., Natraj, V., Nelson, R.R., Osterman, G.B., Payne, V.H., Taylor, T.E., Wunch, D., Drouin, B.J., Oyafuso, F., Chang, A., McDuffie, J., Smyth, M., Baker, D.F., Basu, S., Chevallier, F., Crowell, S.M.R., Feng, L., Palmer, P.I., Dubey, M., García, O.E., Griffith, D.W.T., Hase, F., Iraci, L.T., Kivi, R., Morino, I., Notholt, J., Ohyama, H., Petri, C., Roehl, C.M., Sha, M.K., Strong, K., Sussmann, R., Te, Y., Uchino, O., Velazco, V.A., 2018. Improved retrievals of carbon dioxide from Orbiting Carbon Observatory-2 with the version 8 ACOS algorithm. Atmos. Meas. Tech. 11, 6539–6576. https://doi.org/10.5194/amt-11-6539-2018

https://doi.org/10.5194/essd-2024-315
Preprint. Discussion started: 25 October 2024

Pan, Y., Birdsey, R.A., Fang, J., Houghton, R., Kauppi, P.E., Kurz, W.A., Phillips, O.L., Shvidenko, A., Lewis, S.L., Canadell, J.G., Ciais, P., Jackson, R.B., Pacala, S.W., McGuire, A.D., Piao, S., Rautiainen, A., Sitch, S., Hayes, D., 2011. A Large and Persistent Carbon Sink in the World's Forests. Science 333, 988–993. https://doi.org/10.1126/science.1201609

Parazoo, N.C., Bowman, K., Frankenberg, C., Lee, J.-E., Fisher, J.B., Worden, J., Jones, D.B.A., Berry, J., Collatz, G.J., Baker, I.T., Jung, M., Liu, J., Osterman, G., O'Dell, C., Sparks, A., Butz, A., Guerlet, S., Yoshida, Y., Chen, H., Gerbig, C., 2013. Interpreting seasonal changes in the carbon balance of southern Amazonia using measurements of XCO_2 and chlorophyll fluorescence from GOSAT. Geophys. Res. Lett. 40, 2829–2833. https://doi.org/10.1002/grl.50452

Patra, P.K., Crisp, D., Kaiser, J.W., Wunch, D., Saeki, T., Ichii, K., Sekiya, T., Wennberg, P.O., Feist, D.G., Pollard, D.F., Griffith, D.W.T., Velazco, V.A., De Maziere, M., Sha, M.K., Roehl, C., Chatterjee, A., Ishijima, K., 2017. The Orbiting Carbon Observatory (OCO-2) tracks 2-3 peta-gram increase in carbon release to the atmosphere during the 2014-2016 El Niño. Sci Rep 7, 13567. https://doi.org/10.1038/s41598-017-13459-0

Petzold, A., Thouret, V., Gerbig, C., Zahn, A., Brenninkmeijer, C.A.M., Gallagher, M., Hermann, M., Pontaud, M., Ziereis, H., Boulanger, D., Marshall, J., Nédélec, P., Smit, H.G.J., Friess, U., Flaud, J.-M., Wahner, A., Cammas, J.-P., Volz-Thomas, A., 2016. Global-scale atmosphere monitoring by in-service aircraft – current achievements and future prospects of the European Research Infrastructure IAGOS. Tellus Ser. B-Chem. Phys. Meteorol. 68, 28452. https://doi.org/10.3402/tellusb.v67.28452

Schimel, D.S., 1995. Terrestrial ecosystems and the carbon cycle. Glob. Chang. Biol. 1, 77–91. https://doi.org/10.1111/j.1365-2486.1995.tb00008.x

Schwandner, F.M., Gunson, M.R., Miller, C.E., Carn, S.A., Eldering, A., Krings, T., Verhulst, K.R., Schimel, D.S., Nguyen, H.M., Crisp, D., O'Dell, C.W., Osterman, G.B., Iraci, L.T., Podolske, J.R., 2017. Spaceborne detection of localized carbon dioxide sources. Science 358, eaam5782. https://doi.org/10.1126/science.aam5782

Siabi, Z., Falahatkar, S., Alavi, S.J., 2019. Spatial distribution of XCO_2 using OCO-2 data in growing seasons. J. Environ. Manage. 244, 110–118. https://doi.org/10.1016/j.jenvman.2019.05.049

Silva, S.J., Arellano, A.F., Worden, H.M., 2013. Toward anthropogenic combustion emission constraints from space-based analysis of urban CO_2/CO sensitivity. Geophys. Res. Lett. 40, 4971–4976. https://doi.org/10.1002/grl.50954

Sitch, S., Friedlingstein, P., Gruber, N., Jones, S.D., Murray-Tortarolo, G., Ahlström, A., Doney, S.C., Graven, H., Heinze, C., Huntingford, C., Levis, S., Levy, P.E., Lomas, M., Poulter, B., Viovy, N., Zaehle, S., Zeng, N., Arneth, A., Bonan, G., Bopp, L., Canadell, J.G., Chevallier, F., Ciais, P., Ellis, R., Gloor, M., Peylin, P., Piao, S.L., Le Quéré, C., Smith, B., Zhu, Z., Myneni, R., 2015. Recent trends and drivers of regional sources and sinks of carbon dioxide. Biogeosciences 12, 653–679. https://doi.org/10.5194/bg-12-653-2015

Solomon, S., Plattner, G.-K., Knutti, R., Friedlingstein, P., 2009. Irreversible climate change due to carbon dioxide emissions. Proc. Natl. Acad. Sci. USA 106, 1704–1709. https://doi.org/10.1073/pnas.0812721106

Sundquist, E. T., 1986: Geologic analogs: Their value and limitations in carbon dioxide research. In: The Changing Carbon Cycle [J. R. Trabalka and D. E. Reichle (eds.)], Springer-Verlag, New York, pp. 371–402.

https://doi.org/10.5194/essd-2024-315
Preprint. Discussion started: 25 October 2024

Taylor, T.E., Eldering, A., Merrelli, A., Kiel, M., Somkuti, P., Cheng, C., Rosenberg, R., Fisher, B., Crisp, D., Basilio, R., Bennett, M., Cervantes, D., Chang, A., Dang, L., Frankenberg, C., Haemmerle, V.R., Keller, G.R., Kurosu, T., Laughner, J.L., Lee, R., Marchetti, Y., Nelson, R.R., O'Dell, C.W., Osterman, G., Pavlick, R., Roehl, C., Schneider, R., Spiers, G., To, C., Wells, C., Wennberg, P.O., Yelamanchili, A., Yu, S., 2020. OCO-3 early mission operations and initial (vEarly) XCO_2 and SIF retrievals. Remote Sens. Environ. 251, 112032. https://doi.org/10.1016/j.rse.2020.112032

Taylor, T.E., O'Dell, C.W., Baker, D., Bruegge, C., Chang, A., Chapsky, L., Chatterjee, A., Cheng, C., Chevallier, F., Crisp, D., Dang, L., Drouin, B., Eldering, A., Feng, L., Fisher, B., Fu, D., Gunson, M., Haemmerle, V., Keller, G.R., Kiel, M., Kuai, L., Kurosu, T., Lambert, A., Laughner, J., Lee, R., Liu, J., Mandrake, L., Marchetti, Y., McGarragh, G., Merrelli, A., Nelson, R.R., Osterman, G., Oyafuso, F., Palmer, P.I., Payne, V.H., Rosenberg, R., Somkuti, P., Spiers, G., To, C., Weir, B., Wennberg, P.O., Yu, S., Zong, J., 2023. Evaluating the consistency between OCO-2 and OCO-3 XCO_2 estimates derived from the NASA ACOS version 10 retrieval algorithm. Atmos. Meas. Tech. 16, 3173–3209. https://doi.org/10.5194/amt-16-3173-2023

Taylor, T.E., O'Dell, C.W., Frankenberg, C., Partain, P.T., Cronk, H.Q., Savtchenko, A., Nelson, R.R., Rosenthal, E.J., Chang, A.Y., Fisher, B., Osterman, G.B., Pollock, R.H., Crisp, D., Eldering, A., Gunson, M.R., 2016. Orbiting Carbon Observatory-2 (OCO-2) cloud screening algorithms: validation against collocated MODIS and CALIOP data. Atmos. Meas. Tech. 9, 973–989. https://doi.org/10.5194/amt-9-973-2016

Turnbull, J.C., Tans, P.P., Lehman, S.J., Baker, D., Conway, T.J., Chung, Y.S., Gregg, J., Miller, J.B., Southon, J.R., Zhou, L.-X., 2011. Atmospheric observations of carbon monoxide and fossil fuel CO_2 emissions from East Asia. J. Geophys. Res. Atmos. 116. https://doi.org/10.1029/2011JD016691

Wang, J., Zeng, N., Wang, M., Jiang, F., Chen, J., Friedlingstein, P., Jain, A.K., Jiang, Z., Ju, W., Lienert, S., Nabel, J., Sitch, S., Viovy, N., Wang, H., Wiltshire, A.J., 2018. Contrasting interannual atmospheric CO_2 variabilities and their terrestrial mechanisms for two types of El Niños. Atmos. Chem. Phys. 18, 10333–10345. https://doi.org/10.5194/acp-18-10333-2018

Wang, Y., Yuan, Q., Li, T., Yang, Y., Zhou, S., Zhang, L., 2023. Seamless mapping of long-term (2010–2020) daily global XCO_2 and XCH_4 from the Greenhouse Gases Observing Satellite (GOSAT), Orbiting Carbon Observatory 2 (OCO-2), and CAMS global greenhouse gas reanalysis (CAMS-EGG4) with a spatiotemporally self-supervised fusion method. Earth Syst. Sci. Data 15, 3597–3622. https://doi.org/10.5194/essd-15-3597-2023

Wang, S., Zhang, Y., Ju, W., Chen, J.M., Ciais, P., Cescatti, A., Sardans, J., Janssens, I.A., Wu, M., Berry, J.A., Campbell, E., Fernández-Martínez, M., Alkama, R., Sitch, S., Friedlingstein, P., Smith, W.K., Yuan, W., He, W., Lombardozzi, D., Kautz, M., Zhu, D., Lienert, S., Kato, E., Poulter, B., Sanders, T.G.M., Krüger, I., Wang, R., Zeng, N., Tian, H., Vuichard, N., Jain, A.K., Wiltshire, A., Haverd, V., Goll, D.S., Peñuelas, J., 2020. Recent global decline of CO2 fertilization effects on vegetation photosynthesis. Science 370, 1295–1300. https://doi.org/10.1126/science.abb7772

Wu, L., Hasekamp, O., Hu, H., Landgraf, J., Butz, A., aan de Brugh, J., Aben, I., Pollard, D.F., Griffith, D.W.T., Feist, D.G., Koshelev, D., Hase, F., Toon, G.C., Ohyama, H., Morino, I., Notholt, J., Shiomi, K., Iraci, L., Schneider, M., de Mazière, M., Sussmann, R., Kivi, R., Warneke, T., Goo, T.-Y., Té, Y., 2018. Carbon dioxide retrieval from OCO-2 satellite observations using the RemoTeC algorithm and validation with TCCON measurements. Atmos. Meas. Tech. 11, 3111–3130. https://doi.org/10.5194/amt-11-3111-2018

Wunch, D., Toon, G.C., Blavier, J.-F.L., Washenfelder, R.A., Notholt, J., Connor, B.J., Griffith, D.W.T., Sherlock, V., Wennberg, P.O., 2011. The Total Carbon Column Observing Network. Philosophical Transactions of the Royal Society A: Mathematical, Physical and Engineering Sciences 369, 2087–2112. https://doi.org/10.1098/rsta.2010.0240

Wunch, D., Toon, G.C., Wennberg, P.O., Wofsy, S.C., Stephens, B.B., Fischer, M.L., Uchino, O., Abshire, J.B., Bernath, P., Biraud, S.C., Blavier, J.-F.L., Boone, C., Bowman, K.P., Browell, E.V., Campos, T., Connor, B.J., Daube, B.C., Deutscher, N.M., Diao, M., Elkins, J.W., Gerbig, C., Gottlieb, E., Griffith, D.W.T., Hurst, D.F., Jiménez, R., Keppel-Aleks, G., Kort, E.A., Macatangay, R., Machida, T., Matsueda, H., Moore, F., Morino, I., Park, S., Robinson, J., Roehl, C.M., Sawa, Y., Sherlock, V., Sweeney, C., Tanaka, T., Zondlo, M.A., 2010. Calibration of the Total Carbon Column Observing Network using aircraft profile data. Atmos. Meas. Tech. 3, 1351–1362. https://doi.org/10.5194/amt-3-1351-2010

Wunch, D., Wennberg, P.O., Osterman, G., Fisher, B., Naylor, B., Roehl, C.M., O'Dell, C., Mandrake, L., Viatte, C., Kiel, M., Griffith, D.W.T., Deutscher, N.M., Velazco, V.A., Notholt, J., Warneke, T., Petri, C., De Maziere, M., Sha, M.K., Sussmann, R., Rettinger, M., Pollard, D., Robinson, J., Morino, I., Uchino, O., Hase, F., Blumenstock, T., Feist, D.G., Arnold, S.G., Strong, K., Mendonca, J., Kivi, R., Heikkinen, P., Iraci, L., Podolske, J., Hillyard, P.W., Kawakami, S., Dubey, M.K., Parker, H.A., Sepulveda, E., García, O.E., Te, Y., Jeseck, P., Gunson, M.R., Crisp, D., Eldering, A., 2017. Comparisons of the Orbiting Carbon Observatory-2 (OCO-2) X_{CO2} measurements with TCCON. Atmos. Meas. Tech. 10, 2209–2238. https://doi.org/10.5194/amt-10-2209-2017

Yang, H., Ciais, P., Frappart, F., Li, X., Brandt, M., Fensholt, R., Fan, L., Saatchi, S., Besnard, S., Deng, Z., Bowring, S., Wigneron, J.-P., 2023. Global increase in biomass carbon stock dominated by growth of northern young forests over past decade. Nat. Geosci. 16, 886–892. https://doi.org/10.1038/s41561-023-01274-4

Yoshida, Y., Kikuchi, N., Morino, I., Uchino, O., Oshchepkov, S., Bril, A., Saeki, T., Schutgens, N., Toon, G.C., Wunch, D., Roehl, C.M., Wennberg, P.O., Griffith, D.W.T., Deutscher, N.M., Warneke, T., Notholt, J., Robinson, J., Sherlock, V., Connor, B., Rettinger, M., Sussmann, R., Ahonen, P., Heikkinen, P., Kyrö, E., Mendonca, J., Strong, K., Hase, F., Dohe, S., Yokota, T., 2013. Improvement of the retrieval algorithm for GOSAT SWIR XCO_2 and XCH_4 and their validation using TCCON data. Atmos. Meas. Tech. 6, 1533–1547. https://doi.org/10.5194/amt-6-1533-2013

Yuan, Q., Shen, H., Li, T., Li, Z., Li, S., Jiang, Y., Xu, H., Tan, W., Yang, Q., Wang, J., Gao, J., Zhang, L., 2020. Deep learning in environmental remote sensing: Achievements and challenges. Remote Sens. Environ. 241, 111716. https://doi.org/10.1016/j.rse.2020.111716

Zeng, N., Zhao, F., Collatz, G.J., Kalnay, E., Salawitch, R.J., West, T.O., Guanter, L., 2014. Agricultural Green Revolution as a driver of increasing atmospheric CO_2 seasonal amplitude. Nature 515, 394–397. https://doi.org/10.1038/nature13893

Zeng, Z., Lei, L., Hou, S., Ru, F., Guan, X., Zhang, B., 2014. A Regional Gap-Filling Method Based on Spatiotemporal Variogram Model of CO_2 Columns. IEEE Trans. Geosci. Remote Sens. 52, 3594–3603.

https://doi.org/10.5194/essd-2024-315
Preprint. Discussion started: 25 October 2024

https://doi.org/10.1109/TGRS.2013.2273807

Zhang, M., Liu, G., 2023. Mapping contiguous XCO_2 by machine learning and analyzing the spatio-temporal variation in China from 2003 to 2019. Sci. Total Environ. 858, 159588. https://doi.org/10.1016/j.scitotenv.2022.159588

Zheng, B., Chevallier, F., Ciais, P., Broquet, G., Wang, Y., Lian, J., Zhao, Y., 2020. Observing carbon dioxide emissions over China's cities and industrial areas with the Orbiting Carbon Observatory-2. Atmos. Chem. Phys. 20, 8501–8510. https://doi.org/10.5194/acp-20-8501-2020

Zhou, M., Dils, B., Wang, P., Detmers, R., Yoshida, Y., O'Dell, C.W., Feist, D.G., Velazco, V.A., Schneider, M., De Mazière, M., 2016. Validation of TANSO-FTS/GOSAT XCO_2 and XCH_4 glint mode retrievals using TCCON data from near-ocean sites. Atmos. Meas. Tech. 9, 1415–1430. https://doi.org/10.5194/amt-9-1415-2016